First-Principles Modeling of Protein/Surface Interactions. Polyglycine Secondary Structure Adsorption on the TiO2(101) Anatase Surface Adopting a Full Periodic Approach

First Principles Modeling of Protein/Surface Interactions. Polyglycine Secondary Structure Adsorption on the TiO_2 (101) Anatase Surface Adopting a Full Periodic Approach

Stefano Pantaleone,*[1,2,3] Albert Rimola,*[1] Piero Ugliengo,[2] Mariona Sodupe[1]

[1]*Departament de Química, Universitat Autònoma de Barcelona, Bellaterra 08193, Catalonia, Spain*

[2]*Dipartimento di Chimica and Nanostructured Interfaces and Surfaces (NIS) Inter-Departmental centre, Università degli Studi di Torino, Via P. Giuria 7, 10125 Torino, Italy*

[3]*Dipartimento di Chimica, Biologia e Biotecnologie, Università degli Studi di Perugia, Via Elce di Sotto 8, I-06123 Perugia, Italy*

E-mail corresponding authors:

stefano.pantaleone@unito.it

albert.rimola@uab.cat

Abstract

Computational modeling of protein/surface systems is challenging since the conformational variations of the protein and its interactions with the surface need to be considered at once. Adoption of ab initio methods to this purpose is overwhelming and computationally extremely expensive so that, in many cases, dramatically simplified systems (e.g., small peptides or amino acids) are used, at the expenses of modeling non-realistic systems. In this work we propose a cost-effective strategy for the modeling of

peptide/surface interactions at a full quantum mechanical level, taking the adsorption of polyglycine on the TiO_2 (101) anatase surface as a test case. Our approach is based on the plenty use of the periodic boundary conditions for both the surface model and the polyglycine peptide, giving rise to full periodic polyglycine/TiO_2 surface systems. By proceeding this way, the considered complexes are modelled with a drastically reduced number of atoms compared with the finite-analogous systems, modeling at the same time the polypeptide structures in a realistic way. Within our modeling approach, full periodic DFT calculations (including implicit solvation effects) and ab initio molecular dynamics (AIMD) simulations at the PBE-D2* theory level have been carried out to investigate the adsorption and relative stability of the different polyglycine structures (i.e., extended primary, β-sheet and α-helix) on the TiO_2 surface. It has been found that, upon adsorption, secondary structures become partially denatured because the peptide C=O groups form Ti-O=C dative bonds. AIMD simulations have been fundamental to identify these phenomena because thermal and entropic effects are of paramount importance. Irrespective of the simulated environments (gas phase and implicit solvent), adsorption of α-helix is more favorable than that of β-sheet because in the former more Ti-O=C bonds are formed and the adsorbed secondary structure results less distorted with respect to the isolated state. Under implicit water solvent, additionally, adsorbed β-sheet structures weaken with respect to their isolated states, as the H-bonds between strands are longer due to solvation effects. Accordingly, results indicate that the preferred conformation upon adsorption is the α-helix over the β-sheet.

Introduction

The modeling of protein/surface interactions is a compelling issue for computational chemistry.[1-4] For these cases, in addition to the large conformational variability of the biological partner, the interaction with the solid surfaces also comes into play, inferring an enormous complexity in the considered systems. Because of such a complexity, one can find different strategies to computationally model protein/surface systems. On one hand, there is the use of simplified biological systems, *e.g.*, oligopeptides with a reduced number of residues,[5-10] single amino acids,[11-25] or even amino acid analogues.[26-33] This allows adopting high-quality ab initio methods and to focus on the specific contribution of the various constituting components in the interaction. However, a biological system is not a mere collection of simplified monomers and accordingly this modeling approach overlooks long-ranged and cooperative effects that can greatly contribute to the stability of the protein/surface systems. On the other hand, there is the use of large polypeptides or the actual proteins. However, due to the extremely large size of the systems, the use of ab initio methods is out of reach. Consequently, cheaper but more approximated methods (semi-empirical or force field) must be used, at the expenses of a lower accuracy and, in the case of molecular mechanics-based methods, the inability to cope with bond breaking/making, which may well occur between side chain functionalities and the surfaces. In that respect, force fields need to be tailored to properly describe the specific physical properties and interactions of material surfaces and biological molecules, since models and force fields designed for use in biomolecular simulations are usually not directly transferable to protein/surface simulations. The common types of surface materials in protein–surface computational studies are metal surfaces,[34-37] metal oxides and minerals,[38-42] polymers[43-45] and carbon allotropic surfaces.[46-50]

The interaction between proteins and surfaces is of great relevance in many fields,[51] including bionanotechnology,[52, 53] biomedicine,[54] and biomaterials.[55] Moreover, the interest of this topic is not limited to these applied fields, but it is also of importance in fundamental research as it has implications in prebiotic chemistry and origin of life studies.[56, 57] Indeed, it has been long postulated that mineral surfaces could have played a central role in the synthesis of biopolymers (*e.g.*, polypeptides from amino acid condensation reactions) by catalyzing the processes.[58-61] Additionally, the interaction of polypeptides with naturally-occurring surfaces could have induced their folding into biologically active states, namely, α-helix and β-sheet secondary structures, this way helping to fine tune the machinery that triggered the first biocatalytic reactions needed for the emergence of life.[62-65] Intriguing questions are devoted to know how and why polypeptides change their conformational state upon adsorption, which are related to determine the binding mechanisms and anchoring points present at the interfaces.

Here we present a computational modeling strategy to investigate the interaction of polypeptides with solid-state surfaces. In particular, we present results for the adsorption of a primary extended (*i.e.*, linear polymeric) structure and the secondary (*i.e.*, α-helix and β-sheet) structures of a polypeptide model consisting only of glycine residues (*i.e.*, a polyglycine peptide) on the (101) TiO_2 anatase surface by adopting a full ab initio periodic approach through both static and dynamic electronic structure simulations. The key point of our modeling strategy is to take the advantage of the periodic boundary conditions used to model the surface, which is also applied to the polyglycine peptide model, in such a way that infinite peptide biopolymers folded in different biologically relevant structures are naturally accounted for in the simulations. A similar strategy was originally adopted to model helicoidal conformations of polyglycine chains,[66] and more recently to model the isolated collagen protein with ab-initio methods (using roto-

translational symmetry)[67-70] and its adsorption on hydroxyapatite surfaces.[71] This procedure has allowed us to simulate the adsorption of polyglycine on the surface plenty, *i.e.*, without the need to use simplified or reduced model systems, by describing both short- and long-range interactions consistently and at the same level of accuracy.

TiO_2 is a very attractive material in modern science and technology and is widely used in different fields, including those mentioned above. In nature, three TiO_2 polymorphs can be found: rutile, anatase and brookite. Due to the distinctive catalytic and semiconducting properties of the two former ones, they are the most studied TiO_2 materials as photocatalysts in water splitting to produce green currency of energy (*i.e.*, hydrogen), as assistants in photo degradation of organic molecules for purification and disinfection of wastewater, and as principal components in photovoltaic dye sensitized solar cells.[72] Moreover, due to their chemical stability, non-toxicity and biocompatibility, TiO_2 nanostructures are also used for biomedical purposes,[73] such as being constituents in drug delivery systems and as additive coating materials in orthopedic and dental implants. Additionally, they are currently emerging as new antimicrobial agents, thereby also having potential applications in the antibacterial field. In the particular topic of peptide/surface interactions, it has been shown that TiO_2 nanoparticles can promote the fibrillation of amyloid-β.[74] This phenomenon seems to be correlated with a stabilization of the peptide β-sheet structures,[75] which is the usual secondary structure of polypeptide chains in fibrillary aggregates.[76] Additionally, it has been demonstrated through theory and experiments that TiO_2 can catalyse the formation of peptide bonds between glycine molecules,[77, 78] in which long chain polypeptides (up to 16 monomers) were formed. Moreover, experimental measurements also indicated that the resulting polypeptides adopted helical structures, pointing out a plausible role of TiO_2 in inducing the peptide folding into a bioactive conformation.

By modeling the polyglycine/TiO_2 interactions adopting the above-mentioned strategy, present simulations allow us to provide unique insights on the structure and stability of polyglycine structures once adsorbed on the (101) TiO_2 anatase surface, considering both gas-phase conditions and in the presence of water as solvent (using the PCM implicit solvation model), in which, additionally, we show the relevance to include dynamical effects to actually determine the structural stability of the considered complexes. Overall, the main objective of the present work is to present a consistent, cost-effective strategy to simulate the interactions of secondary structures of a protein with inorganic surfaces. Simulating such interactions is a difficult task and the present methodology overcomes, in part, this difficulty by exploiting the periodicity of the secondary structure. This methodology is shown for polyglycine, the simplest system, but it can be extended to secondary structures with different amino acid composition. Note, however, that a high variability composition will imply a significant increase of computational resources, due to the enlargement of the considered unit cell. Clearly, this methodology would not be applicable, or would not suppose any benefit, to study the adsorption of a whole protein enclosing different secondary structures. Nevertheless, this approach may help disentangle the complex interaction of a real protein with a surface in terms of its subunits, thereby providing new hints on how the adsorption process can occur.

Methods

Modeling polyglycine/TiO_2 complexes

The non-polar TiO_2 (101) anatase surface was modelled as a crystalline periodic slab system, which was constructed by cutting out the TiO_2 anatase bulk structure along the [101] direction (see Figure 1). The cell parameters of the bulk were kept fixed to its

experimental values (a=b=3.784 Å, c=10.239 Å, α=β=γ=90°).[81] The surface slab model consisted of 3 layers of TiO_2 (with a thickness of *ca.* 10 Å), which is the optimum trade-off between accuracy and computational cost.[19] In all the calculations, only the internal positions of the atoms were optimized, keeping the cell parameters fixed. The unit cell used has parameters equal to a=7.569 Å, b=10.239 Å, γ=90°. For some cases a (2x1) supercell-based slab was used because of the size of the polyglycine structures and to avoid fictitious lateral interactions. The c value, which modulates the interlayer distance between replicated slab images, was fixed at 30 Å, thus ensuring an empty space of at least 15 Å among fictitious slab replicas.

As mentioned in the Introduction, the key point to model the polyglycine/TiO_2 complexes by means of a full ab initio periodic approach is that the periodicity adopted to model the slab surface was also adopted to model the polypeptide structures. By proceeding this way, both the extended primary structure and the β-sheet and α-helix secondary structures were also modelled as periodic systems (see Figure 2). For β-sheet structures, in which both parallel and antiparallel conformations have been considered, this modeling strategy was possible by imposing periodicity along both the a and b directions. Periodicity along the former direction served to model a collection of infinite β-strands, while along the latter direction to model the hydrogen bond (H-bond) interactions between strands, in this case established between strands belonging to adjacent unit cells. For the primary extended and α-helix structures, since there are no interactions between structures of adjacent unit cells, periodicity was imposed only through one direction to model the periodic structures. By proceeding this way, the different periodic polyglycine structures were modelled with different glycine units (AA unit) per unit cell: 2 for the extended primary structure, 4 for the β-sheets, and 7 for the α-helices. Such isolated periodic polypeptides were obtained by optimising their periodic

structures using an empty space of 20 Å in the non-periodic directions. In these calculations, both atomic positions and cell parameters were relaxed. Remarkably, this strategy of modeling infinite biopolymeric systems has allowed us to significantly reduce the computational cost of the simulations. Indeed, considering the α-helix as the largest polyglycine structure, only 7 glycine residues per unit cell were needed, a total of 193 atoms if we consider the entire peptide/surface system. In contrast, by modeling a finite (*i.e.*, non-periodic) α-helix structure, at least 12 glycine residues should be used to arrive at reasonable structure, meaning ≈500 atoms that constitute the peptide/surface system.[18] We should bear in mind that an increase of the number of the residues is associated with an increase of the unit cell size of the surface in order to model reasonably well the adsorption, and hence the dramatic increase of the number of atoms in comparison with our approach.

Finally, it is worth mentioning that this "all-periodic" modeling approach used here is possible thanks to the good match between the cell dimensions of the TiO_2 surface model and the isolated periodic polypeptide structures. That is, the unit cell of the extended primary polyglycine system is ≈7.3 Å, which is almost the same value as the *a* parameter of the surface unit cell (*a*=7.569 Å); the unit cell of the β-sheet structures has *a*≈7.3 Å and *b*≈10.1/9.7 Å (parallel/antiparallel conformation), which are very close to the surface unit cell (a=7.569 Å and b=10.23935 Å); finally, the unit cell of the α-helix is ≈10.4 Å, which is very close to the b parameter of the surface unit cell (*a*=15.138 Å and *b*=10. 23935 Å). Only for the α-helix a (2x1) supercell was used, in order to avoid lateral interactions in the non-periodic direction of the α-helix.

Computational details

All periodic calculations were carried out with the Vienna Ab-initio Simulation Package (VASP),[82-85] through which both static quantum mechanical (QM) optimizations and *ab-initio* molecular dynamics (AIMD) simulations were performed. VASP, for the description of the internal ionic cores uses the projector-augmented wave (PAW),[86] while for the valence electrons uses planewaves basis sets. The Perdew-Burke-Ernzerhof (PBE)[87] DFT method in combination with the D2*[88, 89] empirical correction (a modified version of the original Grimme's D2 term for extended systems) to include dispersion forces was adopted as the QM methodology of calculation.

For geometry optimizations, the cut-off energy was set to 500 eV, the self-consistent field (SCF) convergence tolerance to $\Delta E=10^{-5}$ eV, and the tolerance for geometry optimization convergence to 0.01 eV/Å for each atom in any direction. For the systems involving the extended primary and β-sheet structures (i.e., the smallest ones) the k-point mesh was set to (3,3,1), while for those involving the α-helix (i.e., the largest ones) to (2,2,1). In addition to gas-phase, geometry optimizations considering solvent effects have been carried out through the implicit polarizable continuum model (PCM) as implemented in VASP.[90, 91]

Calculation of the vibrational frequencies on the optimized structures were also carried out but only focused on the peptide C=O group. Because of that, a reduced Hessian matrix was built up at the Γ-point by numerical differentiation of the analytical first derivatives using the central difference formula (i.e., two displacements for each atom in each direction), in our case following only the CO displacements. The SCF convergence tolerance in this frequency calculation procedure was set to $\Delta E=10^{-6}$ eV.

For AIMD simulations, the cut-off energy was set to 400 eV and the SCF convergence tolerance to $\Delta E=10^{-5}$ eV. An equilibration period of 1 ps (1000 steps of 1 fs)

in the NVE microcanonical ensemble at the fixed temperature of T=300K was first performed, in which the velocities were scaled at each step. This was followed by a production period of 10 ps in the NVT canonical ensemble, in which the frequency of the temperature oscillation was controlled by the Nosé mass. In order to avoid spurious deformations of the slab structure (since real surfaces are linked to a rigid, macroscopic bulk), only upper atomic layers of the surface model were allowed to move according to the motion's equations for both the equilibration and the production periods, the bottommost atomic layer being at fixed positions.

These adopted computational parameters ensure a full numerical convergence on all the computed properties presented in this work.

Energetics

The adsorption energies of the different polyglycine structures on the TiO_2 (101) anatase surface, both in the gas phase and in implicit PCM water solvent, were calculated as:

$$\Delta E_{ADS} = E_{CPLX}^{(PGLY/\alpha/\beta)} - \left(\frac{M^{(PGLY/\alpha/\beta)}}{N}\right) E_{PGLY} - E_{SURF} \qquad (1)$$

where the notation (PGLY/α/β) indicates the polyglycine structure we refer to (PGLY=extended primary, α=α-helix and β=β-sheet), E_{CPLX} is the total energy of the given polyglycine/surface complex, E_{PGLY} is the total energy of the isolated extended primary polyglycine system, M is the number of AA units of the corresponding adsorbed polyglycine structure in the unit cell, N is the number of AA units of the primary extended structure in the unit cell (*i.e.*, 2), and E_{SURF} is the energy of the isolated surface with the unit cell size adopted for the adsorption of each polyglycine structure (i.e., 1x1 for the adsorption of the extended primary and β-sheet structures and 2x1 for the adsorption of the α-helix structures). By using equation (1), the adsorption energies were computed

taking as peptide of reference the isolated extended primary structure in such a way that all the adsorption energies are referenced from the same system, in this case, the simplest structure. Additionally, by using the isolated extended primary as reference, ΔE_{ADS} accounts for the cost of the cell deformation when the polyglycine interacts with the surface, and on the other hand, the stabilising effects due to the formation of the H-bond interactions defining the α-helix and β-sheets secondary structures.

As the different periodic polyglycine structures were modelled with different amino acidic units (AA units) per unit cell, for a proper comparison between computed adsorption energies, the ΔE_{ADS} values were normalized as a function of the AA units as follows:

$$\Delta E_{ADS/unit} = \frac{\Delta E_{ADS}}{M} \quad (2)$$

where M, as mentioned above, are the number of AA units of each adsorbed polyglycine structure in their unit cell.

Furthermore, we also calculated the energetic gain due to the formation of the H-bond pattern of the secondary structure (α-helix or β-sheet) with respect to the extended primary structure ($\Delta E_{H/unit}$) and the deformation energy of the secondary structures due to the adsorption ($\Delta E_{def/unit}$) as follows:

$$\Delta E_{H/unit} = \left[E_{SGLY}^{(\alpha/\beta)} - \left(\frac{M^{(\alpha/\beta)}}{N}\right) E_{PGLY}\right] \times \frac{1}{M^{(\alpha/\beta)}} \quad (3)$$

$$\Delta E_{def/unit} = \left[E_{SGLY//CPLX}^{(\alpha/\beta)} - E_{SGLY}^{(\alpha/\beta)}\right] \times \frac{1}{M^{(\alpha/\beta)}} \quad (4)$$

where E_{SGLY} is the total energy of the corresponding isolated secondary structure and $E_{SGLY//CPLX}$ is the total energy of the corresponding isolated secondary structure but in their optimized geometry on the surface. The sum of the two terms gives the energy

balance of the H-bond gain and the deformation energy when the polyglycine secondary structures adsorb on the surface with respect to the extended primary structure:

$$\Delta E_{H+def/unit} = \Delta E_{H/unit} + \Delta E_{def/unit} \qquad (5)$$

In the case of the β-sheet/TiO_2 complexes, it is interesting to evaluate all the most important contributions to the total adsorption energy, *i.e.* not only the adsorption energy of the whole β-sheets, but also the adsorption energy of each β-strand with the surface and the interaction energy of the H-bond interactions between the β-strands. The aim is to study the cooperative effects (positive or negative) among the strands. Figure 3 represents schematically a generic β-sheet/TiO_2 complex, which is formed by two β-strands (P1 and P2) per unit cell interacting with the surface (S). This is a common three-body problem, not resolvable analytically. However, to estimate each energy contribution to the total adsorption energy with a good accuracy and shed some light into the likely cooperative effects triggered by the adsorption, we have proceeded as follows. From a given optimized β-sheet/TiO_2 complex, we removed one or two of the three bodies, and performed single-point energy calculations. By proceeding this way, we can decompose the total adsorption energy as: i) $\Delta E_{H\text{-}bond}$, the interaction energy between P1 and P2 without S (*i.e.*, the H-bond contribution), ii) ΔE1, the interaction energy of P1 with S without P2, and iii) ΔE2, the interaction energy of P2 with S without P1. Considering that E_S, E_{P1} and E_{P2} are the single-point absolute energies of the isolated S, P1 and P2 at the optimized β-sheet/TiO_2 complex geometry, respectively, the calculation of each contribution ($\Delta E_{H\text{-}bond}$, ΔE1 and ΔE2) was done as:

$$\Delta E_{H\text{-}bond} = E_\beta - (E_{P1} + E_{P2}) \qquad (6)$$

where E_β is the single-point absolute energy of the β-sheet without S at the optimized β-sheet/TiO_2 complex geometry, and

$$\Delta E1 = E_{P1S} - (E_S + E_{P1}) \quad (7)$$

$$\Delta E2 = E_{P2S} - (E_S + E_{P2}) \quad (8)$$

where E_{P1S} is the single-point absolute energy of the P1/S complex without P2 and E_{P2S} is the single-point absolute energy of the P2/S complex without P1, both cases at the optimized β-sheet/TiO_2 complex geometry.

Finally, we propose a way to assess the capability of the surface to induce peptide folding into a specific secondary structure conformation and, more specifically, if, once the peptide is adsorbed, the interconversion between secondary structures is possible, at least according to the thermodynamics. To know which secondary structure is more stable on the surfaces (i.e., the relative stability between β-sheet and α-helix on the TiO_2 surface), this is possible by comparing the calculated $\Delta E_{ADS/unit}$ values for each complex. That is:

$$\Delta\Delta E_{surf/unit} = \Delta E_{ADS/unit}^{(\beta-PGLY)} - \Delta E_{ADS/unit}^{(\alpha-PGLY)} \quad (9)$$

where $\Delta\Delta E_{surf/unit}$ gives the relative energy between the adsorbed β-sheet and α-helix on, which is obtained by the energy difference between the adsorption energies (per AA unit) of the α-helix and the β-sheet structures (computed using equations 1 and 2 and accordingly referenced from the extended primary structure PGLY). This energy difference arises from the energy cycle shown in Figure 4A, which connects the adsorption energies (per AA unit) of the isolated extended primary structure on the surface with the α-helix/TiO_2 → β-sheet/TiO_2 conversion process. Note that this direct energy difference is only possible using the normalized adsorption energy values, as the β-sheet/TiO_2 and α-helix/TiO_2 systems have different AA units in the periodic structure and they are adsorbed on different surface unit cells. However, this straightforward calculation does not provide any information on the energy cost involved in the

conversion process. To have deeper insights onto that, we build up the energetic cycle shown in Figure 4B, in which the conversion from the α-helix/TiO_2 to the β-sheet/TiO_2 complexes is decomposed in three steps: i) desorption of the α-helix from the surface to be in its isolated state, ii) conversion of the isolated α-helix into β-sheet, and iii) adsorption of the isolated β-sheet on the surface. Each step is associated with an energy cost/gain, the global balance indicating if the process is favourable or not. According to the cycle, the reaction energy for the conversion of α-helix/TiO_2 → β-sheet/TiO_2 can be expressed as:

$$\Delta\Delta E_{surf/unit} = \Delta E^{(\beta)}_{ADS/unit} - \Delta E^{(\alpha)}_{ADS/unit} + \Delta\Delta E_{iso/unit} \quad (10)$$

where $\Delta E^{(\beta)}_{ADS/unit}$ and $\Delta E^{(\alpha)}_{ADS/unit}$ are the adsorption energies (per AA unit) of the β-sheet and α-helix structures, respectively, on the TiO_2 surface from their corresponding isolated states, that is:

$$\Delta E^{(\alpha/\beta)}_{ADS/unit} = \left[E^{(\alpha/\beta)}_{CPLX} - E^{(\alpha/\beta)}_{SGLY} - E^{(\alpha/\beta)}_{SURF}\right] \times \frac{1}{M^{(\alpha/\beta)}} \quad (11)$$

and $\Delta\Delta E_{iso/unit}$ is the energy associated with the α-helix → β-sheet conversion for the secondary structures in their isolated states, i.e.,

$$\Delta\Delta E_{iso/unit} = \frac{E^{(\beta)}_{SGLY}}{M^{(\beta)}} - \frac{E^{(\alpha)}_{SGLY}}{M^{(\alpha)}} \quad (12)$$

in which the total energies are normalized by the AA units of each structure, i.e., $M^{(\beta)}$=4 and $M^{(\alpha)}$=7. Remarkably, the $\Delta\Delta E_{surf/unit}$ term, irrespective of being computed through equation (9) or equation (10), the result must be the same. For the sake of completeness, more detailed expressions of equations (9), (10), (11) and (12) are provided in SI.

Results and Discussion

The TiO_2 (101) anatase surface model exhibits pentacoordinated Ti atoms (Ti_{5c}) placed at the outermost positions of the slab (see Figure 1). Since these Ti_{5c} atoms are coordinatively unsaturated they can act as acidic Lewis sites and, accordingly, they are prone to establish covalent dative bonds with lone pairs as those provided by N and O terminal atoms. Additionally, the surface also presents bivalent "bridge" O atoms (O_{br}), which bonds two surface Ti_{5c} atoms (see Figure 1). These O_{br} atoms can act as basic Lewis sites, enabling the formation of H-bond interactions with adsorbate species. These adsorbent properties of the surface are particularly appealing when dealing with the adsorption of the polyglycine structures, since polyglycine presents chemical groups that can interact with the surface through these interactions, in particular H-bonds with the peptide N-H groups, and dative bonds with peptide C=O groups. Interestingly, the same NH and CO moieties interact one to each other defining the secondary structure. Therefore, one can expect a competitivity between the internal N-H/CO interactions of the peptide with the surface, which, depending on the surface composition and morphology, may lead to a specific folding of the adsorbed peptide.

Extended primary structure

The simplest polyglycine conformation is its extended primary structure forming a linear polymer. The complex of this structure in interaction with the TiO_2 (101) anatase surface (shown in Figure 5) will be named along the work as extended/TiO_2 complex. As mentioned above, this primary structure was modelled within a periodic framework by repeating 2 amino acidic units along the *a* direction of the unit cell. The biopolymer interacts with the surface through a Ti—O dative bond, with ΔE_{ADS} = -62.0 kJ mol^{-1} and $\Delta E_{ADS/unit}$= -31.0 kJ mol^{-1} (see Table 1). However, by accounting for solvent effects, these adsorption energy values drop down to ΔE_{ADS} = -3.8 kJ mol^{-1} and $\Delta E_{ADS/unit}$= -1.9

kJ mol^{-1} (see Table 1). In general, inclusion of implicit solvation leads to a significant decrease of the adsorption energies. This is because, in order that the solvated peptide and the solvated surface interact, many interactions with the solvent are lost, hence presenting an energetic cost, which is only partly covered by the newly formed favorable interactions between the two interacting partners. From the point of view of structural changes, inclusion of implicit solvent does not affect the extended primary structure, both the periodic isolated and extended/TiO_2 complex (see Figure 2 and Figure 5).

This very simple system is enough to observe that interaction with the surface induces structural changes on the peptide structure. Indeed, in absence of the surface, the distances between two adjacent C=O/N—H groups (which we can understand as a weak H-bond) are ≈2.08 Å (see Figure 2). On the surface, the distances increase to ≈2.32/2.35 Å and accordingly the adsorption weakens this interaction. In order to investigate this significant structural change once the extended polyglycine adsorbs on the surface, additional optimizations were run for the isolated extended primary polyglycine, in which the periodic cell parameter was fixed to that of the TiO_2 surface. The computed values for the C=O/N—H distances are now ≈2.29 Å (see Figure S3 and Table S1 of SI). Thus, although adsorption leads to an increase of these distances, these results show that the main contribution to the polyglycine deformation upon adsorption arises from the fact that the polypeptide needs to adapt its unit cell to the different cell size of TiO_2.

β-sheet structures

The first secondary polyglycine structure analysed in this work is the β-sheet, both in its parallel and antiparallel conformations (hereafter referred to as β-sheet_P and β-sheet_AP, respectively). The isolated periodic structures are shown in Figure 2. In β-

sheet_AP, the two β-strands run in opposite directions, so that the N-terminus of one β-strand is adjacent to the C-terminus of the other. In contrast, in β-sheet_P, the two β-strands run in the same direction and accordingly the N-terminus of one β-strand is on the other side with respect to the N-terminus of the other β-strand. Due to these dispositions of the N- and C- termina, in β-sheet_AP the H-bonds are aligned directly opposite to each other, while in β-sheet_P the geometry of the individual glycine residue forces the H-bond to occur at an angle. Thus, H-bonds in β-sheet_AP are stronger and more stable than in β-sheet_P.

Figure 6 shows the optimized structures of the β-sheet_AP/TiO_2 and β-sheet_P/TiO_2 complexes. In both systems, one β-strand interacts with the surface via a Ti—O dative bond, while the other through dispersive forces, since neither Ti-O nor H-bond interactions are established.

By comparing the structures of the isolated β-sheets with those on the surface, for both β-sheet conformations, adsorption induces an increase of the H-bond distances (2.097 – 2.098 Å vs 2.297 – 2.587 Å for the AP cases and 2.621 – 2.622 Å vs 2.668 – 2.802 Å for the P cases), and even the breaking of H-bonds for those C=O groups involved in the formation of Ti—O dative bonds. Therefore, although the weakening, the H-bond pattern in β-sheet_AP/TiO_2 remains stronger than in β-sheet_P/TiO_2 and the former complex presents a higher adsorption energy than the latter (ΔE_{ADS} = -120.8 and -115.7 kJ mol^{-1} and $\Delta E_{ADS/unit}$ = -30.2 and -28.9 kJ mol^{-1}, respectively). Interestingly, the difference in the $\Delta E_{ADS/unit}$ between the two β-sheet conformations (1.3 kJ mol^{-1}) is lower than the difference in the energetic gain of the β-sheets with respect to the extended structure, (5.1 kJ mol^{-1}, as $\Delta E_{H/unit}$ = -23.6 and -18.5 kJ mol^{-1} for the antiparallel and parallel β-sheets, respectively, see Table 1), meaning that the stability of the two β-sheets is more similar upon adsorption than in their isolated states. This is due to the lower

deformation energy of β-sheet_P ($\Delta E_{def/unit}$ = 19.6 kJ mol^{-1}) with respect to the β-sheet_AP ($\Delta E_{def/unit}$ = 23.0 kJ mol^{-1}) in the complexes because the cell parameters of the former are closer to those of the surface.

As mentioned in the Computational Details section, by performing single-point energy calculations on the β-sheet/TiO_2 complexes, we decomposed the single energetic contributions to the total adsorption energy (see Figure 3). We name P1 as the β-strand bound to the surface via Ti—O dative bond and P2 as the β-strand bound via dispersive forces. Accordingly, we have calculated ΔE1, *i.e.* the interaction of P1 with the surface (without P2), ΔE2, *i.e.* the interaction of P2 with the surface (without P1), and $E_{H\text{-}bond}$, *i.e.* the energy of the H-bond pattern (without the surface). All data are calculated as single points at the geometry of the complex and presented in Table 2. As expected, $E_{H\text{-}bond}$ is larger for β-sheet_AP than for β-sheet_P, and ΔE1 is larger than ΔE2. To check whether the β-sheet adsorption is accompanied by positive or negative cooperative effects, we compared the sum of all the energies of the systems separately and their corresponding interactions, *i.e.* $E_{CALC} = E_{P1} + E_{P2} + E_S + \Delta E1 + \Delta E2 + \Delta E_{H\text{-}bond}$, with the actual total energy of the complexes E_{TOT} (as computed by VASP). The analysis indicates that E_{TOT} is slightly higher than E_{CALC}, thus showing a minor negative cooperativeness, meaning that there is some competitiveness among the three bodies.

It is worth mentioning that, for some cases, the β-sheet secondary structure adsorbed on the surface is strongly affected by implicit solvent. As said above, the H-bond pattern becomes weaker by the adsorption, and, because of the larger distance among the strands, screening effects by the solvent are more effective, which further increases the distance between them (increments up to 0.4 Å). Calculated adsorption energies ($\Delta E_{ADS/unit}$ = -0.1, -0.9 and -4.1 kJ mol^{-1}, for β-sheet_AP/TiO_2, β-sheet_P/TiO_2

and β-sheet_BRK/TiO_2, respectively, see Table 1) strongly decrease with respect to the gas-phase calculations ($\Delta E_{ADS/unit}$ = -30.2, -28.9 and -30.8 kJ mol^{-1}).

Finally, in view of the large $\Delta E_{ADS/unit}$ shown by the extended/TiO_2 complex due to the Ti-O dative bonds (see above), we have carried out AIMD simulations on both β-sheet/TiO_2 complexes to check if transformation from the β-sheets to the extended structure takes place by rotation of the two strands with respect to the normal surface, enabling a new Ti-O dative bond in the P2 strand. However, AIMD simulations indicate that both systems prefer to maintain the H-bond patterns rather than establishing additional Ti—O bonds (see Figures S4 and S5 of SI). In view of that, from the β-sheet_AP/TiO_2 complex, we have manually built a structure in which the peptide adopts a primary-like conformation by rotating the two β-strands (hereafter named as β-sheet_BRK/TiO_2, see Figure 6A). The optimized resulting structure for β-sheet_BRK/TiO_2 is slightly more favourable than β-sheet_AP/TiO_2 and β-sheet_P/TiO_2 (ΔE_{ADS} = -123.2 kJ mol^{-1} and ΔE_{ADS}/unit = -30.8 kJ mol^{-1}). To check the stability of β-sheet_BRK/TiO_2 accounting for dynamical effects, we have executed AIMD simulations to assess the evolution of this structure over time (see Figure 7B and 7C). Following the evolution of the O—H and Ti—O distances, since the very first step of the simulation, the two strands rotate to restore the β-sheet_AP conformation. Therefore, we can conclude that, despite that potential energy values indicate β-sheet_AP/TiO_2 as less stable than β-sheet_BRK/TiO_2 (2.4 kJ mol^{-1}), when thermal and entropic effects are accounted for, the β-sheet_AP structure adsorbed on the surface is found to be the most stable complex. However, when AIMD simulations are carried out in PCM (AIMD-PCM), the β-sheet_BRK/TiO_2 complex is maintained along the whole simulation (see Figure S6), in line with static PCM calculations, indicating that this configuration, more exposed to the solvent, becomes stabilized when solvent effects are included. AIMD-PCM simulations

of the β-sheet_AP/TiO_2 complex (see Figure S7) also show that the peptide remains attached on the surface keeping their secondary structures. Note, however, that the structures present higher root mean square deviations (RMSD) with respect to the gas phase because the solvent competes with the mutual interaction of the β-strands and with the surface.

α-helix structures

The other very common secondary structure found in proteins is the α-helix. The α-helix structure presents typically $i + 4 \rightarrow i$ H-bonds. That is, the NH group of one residue forms a H-bond with the C=O group belonging to fourth previous residues (see the isolated periodic structure of the polyglycine α-helix in Figure 2). Figure 8A shows the optimized structure of the α-helix on the TiO_2 (101) anatase surface (hereafter referred to as α-helix_1/TiO_2). As one can see in this complex, the periodicity along the *b* direction of the surface unit cell has been used to model the infinite α-helix. By comparing the isolated α-helix with that adsorbed on the surface, the main structural change is the breaking of one H-bond due to the formation of a Ti—O bond. The rest of H-bonds are not significantly altered due to the surface interaction, being around 1.86 – 1.87 Å. The calculated adsorption energies are ΔE_{ADS} = -220.1 kJ mol^{-1} and $\Delta E_{ADS/unit}$ = -31.5 kJ mol^{-1}, very similar to the values obtained for the extended/TiO_2 and β-sheet_AP/ TiO_2 complexes.

In the presence of implicit solvent, the energetics for the α-helix complexes follow the same trend as for the other structures, i.e. the adsorption energy decreases with respect to gas phase conditions (ΔE_{ADS} = -80.8 kJ mol^{-1} and $\Delta E_{ADS/unit}$ = -11.5 kJ mol^{-1}). However, at variance with the β-sheets structures, the H-bond pattern does not undergo

significant distortions. This is because most of the H-bonds are not affected by the presence of the surface and accordingly, the solvent cannot "interpose" between the H-bond groups as it happens for β-sheets, this way the H-bonds remaining almost unaltered by the presence of solvent.

In view of the relevance to include dynamic effects in the β-sheet/TiO_2 complexes, AIMD simulations have been also carried out for the α-helix_1/TiO_2 complex. During the simulations, one can identify some denaturation of the peptide; *i.e.* the α-helix structure is partly lost (see Figure 9). Indeed, new Ti-O dative bonds are formed, at expenses to break the $i + 4 \rightarrow i$ H-bonds close to the surface. Due to that, the NH groups involved in the broken $i + 4 \rightarrow i$ H-bonds lead to form a $i + 5 \rightarrow i$ H-bond; that is, the NH establishes a H-bond with a C=O group five residues earlier, with a H-bond distance of about 2.7 Å. Because of the formation of the new Ti—O bond, we have chosen the last snapshot of the AIMD simulation as the initial structure for a new geometry optimization. The optimized structure is shown in Figure 8B (α-helix_2/TiO_2), which indeed presents the different Ti-O bonds and both $i + 4 \rightarrow i$ and $i + 5 \rightarrow i$ H bond patterns. The calculated adsorption energy for α-helix_2/TiO_2 (ΔE_{ADS} = -235.9 kJ mol^{-1} and $\Delta E_{ADS/unit}$ = -33.7 kJ mol^{-1}) is larger than for α-helix_1/TiO_2 (ΔE_{ADS} = -220.5 kJ mol^{-1} and $\Delta E_{ADS/unit}$ = -31.5 kJ mol^{-1}), indicating that this structure is more stable on the surface, although the helix structure is more distorted. Interestingly, calculated $\Delta E_{H/unit}$ values are the same for α-helix_1/TiO_2 and α-helix_2/TiO_2 complexes, indicating that in both complexes the energy gain due to the formation of the helix structure is the same even on the surface, irrespective its distortion on the surface. However, AIMD-PCM simulations converts the α-helix_2/TiO_2 complex into α-helix_1/TiO_2 during the very first part of the equilibration (see Figure S8), i.e., it passes from exhibiting two Ti-O dative bonds (per unit cell) to only one. This is in line with PCM static calculations as α-helix_1/TiO_2 results to be

slightly more stable than α-helix_2/TiO_2 (see Table 1). After 3 picoseconds (see Figure S8) also the last Ti-O dative bonds is lost and the helix fully restores its H-bond pattern, the interaction with the surface being only through dispersive forces. Furthermore, we want to highlight that, despite the Ti-O distances continuously increase during the simulation, this does not mean that the helix desorbs from the surface. This simply reflects that the helix is moving on the surface due to the decreasing number of dative bonds as anchoring points.

CO frequency calculations.

The stretching vibration of the peptide C=O bonds, ν(CO), is an interesting property to analyze, since it can be experimentally traced by infrared spectroscopy. Indeed, free peptide C=O groups present an intense stretching vibrational band at about 1600-1700 cm^{-1}. This region of the IR spectrum is usually clean so that ν(CO) IR band does not overlap with other vibrational frequencies. Accordingly, it is used as a fingerprint reference mode frequency in C=O-containing molecules; in experimental measurements, the hypsochromic/bathochromic shifts in the C=O stretching frequency allow to figure out the kind of interaction with the surrounding (either surfaces or other molecules). In our polyglycine/TiO_2 systems, two main features can perturb the ν(CO) values: i) the H-bond interactions with N—H groups involved in the secondary structures, and ii) the dative interactions of the CO group with Ti_{5c} atoms. It is worth mentioning that the PBE functional underestimates the absolute value of the vibrational stretching frequencies, so that our values are down-shifted by 50/60 cm^{-1} with respect to the experimental values. Simulated IR spectra centered to the ν(CO) region of the polyglycine structures, for both the periodic isolated and adsorbed on the TiO_2 surface, are shown in Figure 10. Computed values are reported in Table S3 of SI.

In the isolated extended primary structure, calculated ν(CO) are 1655 and 1622 cm^{-1}. This extended peptide has two independent C=O groups (one per glycine residue in the unit cell) but the ν(CO) motions are coupled since the first and second ν(CO) values correspond to the antisymmetric and symmetric stretching modes, respectively. As expected, on the TiO_2 surface, these values are bathochromic -shifted to 1599 and 1619 cm^{-1} due to the Ti_{5c}-OC bonds.

Experimentally, β-sheet systems present two ν(CO) bands at 1685 and 1629 cm^{-1}. In our isolated β-sheet structures, the ν(CO) values are bathochromic shifted with respect to the values of the extended primary structure due to the H-bonds between the β-strands. In the antiparallel conformation the ν(CO) frequency range is 1656 – 1578 cm^{-1}, while in the parallel one is 1650 – 1592 cm^{-1}, in agreement with the stronger H-bond interactions in the former. When the β-sheets are adsorbed on the surface, a bathochromic shift of all the ν(CO) modes is observed. The bathochromic shift is particularly important for C=O groups engaged in the Ti_{5c}-O bonds with the surface: for instance, in β-sheet_AP/TiO_2, the frequency at 1578 cm^{-1} moves to 1547 cm^{-1} ($\Delta\nu$ = -31 cm^{-1}) and in β-sheet_AP/TiO_2 the frequency at 1592 cm^{-1} moves to 1544 cm^{-1} ($\Delta\nu$ =- 48 cm^{-1}).

In the isolated α-helix system, an overall bathochromic shift of the ν(CO) values with respect to the values of the extended primary structure is computed due to the H-bond pattern defining the helical structure. In the α-helix_1/TiO_2, the frequency of the C=O group involved in the Ti_{5c}-O bonds passes from 1611 cm^{-1} to 1558 cm^{-1} ($\Delta\nu$ = -53 cm^{-1}). However, for the remaining ν(CO) vibration frequencies both bathochromic and hypsochromic shifts are computed. We attribute this behavior to the breaking of the homogeneous α-helical content upon adsorption. In the isolated α-helix, the H-bond distances involving the C=O groups, range from 1.866 up to 1.872 Å, whereas when adsorbed on the TiO_2 surface the range increases from 1.754 up to 1.916 Å. Therefore,

the C=O frequency shifts are modulated by the hydrogen bond features. For instance, the highest ν(CO) frequency mode (1679 cm^{-1}) is associated to the longest H-bond (1.916 Å). In the α-helix_2/TiO_2 system, the ν(CO) frequency values of the C=O involved in the Ti_{5c}-O bonds are close to those for the C=O groups involved in simultaneous $i + 4 \rightarrow i$ and $i + 5 \rightarrow i$ H-bond patterns (1599 cm^{-1} and 1601 cm^{-1}, respectively). Therefore, the electronic effect on the peptide C=O bond interacting with the Ti_{5c} atoms is similar to that involved in the two H-bond patterns. The highest ν(CO) frequency (1662 cm^{-1}) is indeed associated to a C=O neither involved in Ti_{5c}-O bonds nor in H-bonding with the N—H groups (see Figure 7B).

The vibrational frequencies have also been computed within the PCM solavtion model. Results (reported in Table S3) indicate that, as a major trend, PCM frequencies decrease compared to the values computed in the gas phase; however, the decrease is similar for both the isolated systems and the adsorbed cases. This is the consequence of the solvent dielectric continuum screening weaking the chemical bonds in the same way, irrespective if the secondary structures are isolated or adsorbed.

Stability between secondary structures

Table 3 shows the results on the relative stability of α-helix and β-sheet in their isolated states and on the TiO_2 surface in both gas phase and in PCM water phase, according to the energy cycle presented in the Computational Details section. The conformational change process defined by the cycle is the α-helix → β-sheet conversion. Accordingly, negative values indicate that conversion into β-sheet is favorable, and vice versa.

Among the studied systems, in the gas phase, the isolated β-sheet_AP structure is the most stable conformation, more than the α-helix ones. In contrast, upon adsorption, also in the gas phase, the α-helix conformation is more favorable than the β-sheet ones. This is also reflected by the ΔE_{ADS}/unit values, the α-helix_2/ TiO_2 complex presenting the largest value (-33.7 kJ mol^{-1}) compared with the β-sheet_P/TiO_2 and β-sheet_AP/TiO_2 complexes (-30.2 kJ mol^{-1} and -28.9 kJ mol^{-1}). Accordingly, a polyglycine system adsorbed on the TiO_2 (101) anatase surface prefers the α-helix folding rather than the β-sheet one under gas-phase conditions. Moreover, the α-helix_1/TiO_2 complex also presents a higher $\Delta E_{ADS/unit}$ (-31.5 kJ mol^{-1}) than the β-sheet complexes, strengthening even more the α-helix preference upon adsorption.

When implicit solvation effects are accounted for, the isolated β-sheet_AP and the α-helix structures present almost the same stability, since the reaction energy conversion adopting the energy cycle results in 0.8 kJ mol^{-1} (below the chemical accuracy). In contrast, in the presence of the TiO_2 surface, significant reaction energy values are obtained (between 11-12 kJ mol^{-1}), clearly indicating that, under these conditions, adsorbed α-helices are more stable than β-sheets. This is probably due to the weakening of the β-sheet H-bond pattern caused by the solvation, while this is not the case for α-helices. Thus, these results point out that, on the TiO_2 surfaces and in implicit PCM water solvent, the α-helix is further stabilized upon adsorption with respect to the β-sheet.

The present simulations do not account for the role of explicit water molecules. This is particularly relevant when specific interactions, like H-bond interactions, are present as in the present case (*vide supra*).. To estimate the role of explicit water solvation, a water monolayer is adsorbed on all the outermost Ti_{5c} atoms.The computed adsorption energies are reported in Figure S9 and Table S4 of SI. The solvated TiO_2 was

then computed adopting the PCM scheme. This scheme allows to describe the local specific interactions by explicit water molecules, delegating the long range solvent effect to the PCM Adsorbed water molecules do not dissociate, in agreement with previous calculations by some of us.[92] To calculate the adsorption energy, we have taken, as a reference systems, the isolated extended primary structure, for the biological part, plus the solvated surface, both treated with PCM. As a general trend, results indicate that the adsorption is slightly more favorable when the surface is saturated by explicit water molecules than for the bare surface, thereby suggesting that adsorption may be water-mediated. Remarkably, the trend that α-helix adsorbs more favorably than β-sheet is confirmed, irrespective of the degree of solvation, indicating that the insights provided by the static calculations are somehow reliable.

It is worth mentioning that entropy effects may also play a role in the α-helix → β-sheet interconversion. For polypeptides without side chains (like the polyglycines adopted in this work), loss of the backbone entropy is expected to disfavour the α-helix configuration as compared to the β-sheet. Nevertheless, considering the larger adsorption energy of the α-helix on TiO_2, we expect this configuration to be the preferred one at this surface. For other polypeptides, side chains conformational entropy losses can also play a role, the final stability being determined not only by the secondary structure[94] but also by how side chains interact with the surface. Clearly, this matter is difficult and merits further study to be carried out in the future.

Conclusions

In the present work, the adsorption and stability of primary (linearly extended) and secondary (β-sheet and α-helix) peptide structures, here using polyglycine as a

peptide model, on the TiO_2 (101) anatase surface have been theoretically studied with periodic simulations at the DFT(PBE)-D2* level by performing static geometry optimizations and AIMD simulations, both in the gas phase and in PCM implicit water solvent). A crucial point to model the polyglycine/TiO_2 interactions in a computationally affordable way without penalizing the reliability of the peptide structures has been the application of the periodic boundary conditions to both the surface and the polyglycine, this way obtaining infinite biopolymeric peptide structures adsorbed on the TiO_2 surface.

For a proper comparison among the adsorption of the different polyglycine structures, calculated adsorption energies have been normalized per glycine unit (*i.e.* $\Delta E_{ADS/unit}$), since each structure requires different units to be realistic enough, namely, 2 for the extended primary, 4 for β-sheet and 7 for α-helix. The academic case of the adsorption of the extended primary structure indicates that the peptide C=O groups are prone to form covalent dative bonds with surface Ti_{5c} atoms. For β-sheet and α-helix, the adsorption presents a delicate trade-off between keeping the H-bond pattern of the secondary structures and forming the Ti-O bonds.

Among the different considered complexes, the α-helix ones have been found as the most stable ones in all the different simulated environments (gas phase, implicit and explicit water solvent), the only difference between gas phase and implicit solvation being the number of Ti-O dative bonds (two in α-helix_2/TiO_2, one in α-helix_1/TiO_2). Remarkably, AIMD simulations were useful to identify the α-helix_2/TiO_2, the most stable complex in gas phase, where the formation of the second Ti-O dative bond along the evolution of the system was observed. AIMD-PCM simulations confirm the results obtained with static PCM calculations, *i.e.,* starting from the α-helix_2/TiO_2, it converts into α-helix_1/TiO_2, which is more stable in PCM. For the adsorption of the β-sheet structures, considering only potential energy values, the β-sheet_BRK/TiO_2 complex is

the most stable ($\Delta E_{ADS/unit}$ = -30.8 (-4.1 in PCM) kJ mol^{-1}), closely followed by β-sheet_AP/TiO_2 ($\Delta E_{ADS/unit}$ = -30.2 (-0.1 in PCM) kJ mol^{-1}). The difference between these two complexes is that the former presents two Ti-O bonds at expenses to break several H-bond interactions, partially disrupting the β-sheet structure, while in the latter, only one Ti—O dative bond is present, thus keeping the β-sheet structure in place. However, irrespective of the tiny energetic difference between these two complexes, AIMD simulations taking β-sheet_BRK/TiO_2 as the initial guess structure clearly show the conversion from this complex to β-sheet_AP/TiO_2, thus indicating that β-sheet_BRK/TiO_2 is not stable at 300 K, thus favoring the β-sheet_AP/TiO_2 complex. In constrast, β-sheet_BRK/TiO_2 is stable during AIMD-PCM simulations, as also predicted by static calculations. As a general trend the RMSD during the AIMD-PCM simulations is larger with respect to the gas phase, indicating that water strongly compete with the surface in the interaction with the peptide. This is also confirmed by the presence of a monolayer of explicit water molecules attached to the most exposed surface Ti ions, suggesting a possible water-mediated protein/TiO_2 adsorption.

Upon detailed analysis of the computed adsorption energies both in gas phase and in PCM by adopting an energy cycle, results point out that α-helix is the preferred secondary structure conformation over β-sheet to adsorb on the TiO_2 (101) anatase surface.

Finally, the peptide C=O vibrational stretching mode has been calculated for all the structures, in both their isolated and adsorbed states. The red-/blue-shifts undergone by the ν(CO) because of the adsorption have been analysed and interpreted from an atomistic perspective. The same calculations performed in PCM show that water (even modelled with an implicit solvent) affects the results by bathochromically shifting the gas

phase ν(CO) calculated frequencies. These vibrational data can guide the interpretation of the infrared spectroscopy measurements apt to elucidate the TiO_2-induced peptide folding.

The computational approach here proposed to model peptide/surface interactions has been applied in the present work only for a polyglycine peptide model on the (101) anatase surfaces. However, it can also be extended to other polypeptides systems, this way opening up a fertile ground to study the adsorption of more realistic polypeptide systems (i.e., containing different amino acidic residues) on the same surface, which will be useful to check the stability and possible conformation variations (even conversions) of their secondary structures upon adsorption.

Data and Software Availability

All the simulations have been performed with the Vienna Ab-initio Simulation Package (VASP) commercial code (https://www.vasp.at), version 5.2. Visualization and manipulation of the structures have been carried out with the MOLDRAW package (https://www.moldraw.unito.it) and figures rendered with the POVRAY program (http://www.povray.org/), both codes being publicly available software.

All the data published in this work is available free of charge as Supporting Information.

- Energy diagrams for the conversion of α-helix/TiO_2 → β-sheet/TiO_2 and expressions to compute the reaction energy; Optimized geometries of the isolated periodic extended primary polyglycine structure using the cell parameters of the TiO_2 (101) anatase surface; Evolution of the H-bonds and Ti-O bonds along the ab initio molecular dynamics simulations for the β-sheet_AP/TiO_2 and β-

sheet_P/TiO_2 complexes; cell parameters of the computed periodic systems; relative energies (in kJ/mol) of the α-helix → β-sheet conformational change and related energetic terms; vibrational C=O stretching for all the polyglycine/TiO_2 systems studied.

- Optimized fractionary coordinates and cell parameters of all the simulated periodic structures.

Acknowledgments

The authors gratefully acknowledge financial support from MINECO (Project CTQ2017-89132-P) and DIUE (Project 2017SGR1323). A.R. is indebted to the "Ramón y Cajal" program. S.P. and P.U. acknowledge the Italian Space Agency for co-funding the Life in Space Project (ASI N. 2019-3-U.O). BSC-MN is kindly acknowledged for the generous allowance of computing time through the QCM-2017-1-0027 and QCM-2017-2-0016 projects "Ab initio modeling of protein-surface interactions. Stability of peptide secondary structures upon adsorption on TiO_2 surfaces".

References

1. Di Felice, R.; Corni, S., Simulation of Peptide–Surface Recognition. *J. Phys. Chem. Lett.* **2011,** *2*, 1510-1519.
2. Latour, R. A., Molecular simulation of protein-surface interactions: Benefits, problems, solutions, and future directions (Review). *Biointerphases* **2008,** *3*, FC2-FC12.
3. Praprotnik, M.; Site, L. D.; Kremer, K., Multiscale Simulation of Soft Matter: From Scale Bridging to Adaptive Resolution. *Ann. Rev. Phys. Chem.* **2008,** *59*, 545-571.
4. Ozboyaci, M.; Kokh, D. B.; Corni, S.; Wade, R. C., Modeling and simulation of protein–surface interactions: achievements and challenges. *Q. Rev. Biophys.* **2016,** *49*, e4.
5. Muir, J. M. R.; Costa, D.; Idriss, H., DFT computational study of the RGD peptide interaction with the rutile TiO2 (110) surface. *Surf. Sci.* **2014,** *624*, 8-14.
6. Lee, S.-S.; Kim, B.; Lee, S., Structures and Bonding Properties of Gold–Arg-Cys Complexes: DFT Study of Simple Peptide-Coated Metal. *J. Phys. Chem. C* **2014,** *118*, 20840-20847.

7. Rimola, A.; Aschi, M.; Orlando, R.; Ugliengo, P., Does Adsorption at Hydroxyapatite Surfaces Induce Peptide Folding? Insights from Large-Scale B3LYP Calculations. *J. Am. Chem. Soc.* **2012,** *134*, 10899-10910.
8. Calzolari, A.; Cicero, G.; Cavazzoni, C.; Di Felice, R.; Catellani, A.; Corni, S., Hydroxyl-Rich β-Sheet Adhesion to the Gold Surface in Water by First-Principle Simulations. *J. Am. Chem. Soc.* **2010,** *132*, 4790-4795.
9. Schneider, J.; Colombi Ciacchi, L., Specific Material Recognition by Small Peptides Mediated by the Interfacial Solvent Structure. *J. Am. Chem. Soc.* **2012,** *134*, 2407-2413.
10. Akdim, B.; Pachter, R.; Kim, S. S.; Naik, R. R.; Walsh, T. R.; Trohalaki, S.; Hong, G.; Kuang, Z.; Farmer, B. L., Electronic Properties of a Graphene Device with Peptide Adsorption: Insight from Simulation. *ACS Appl. Mater. Interf.* **2013,** *5*, 7470-7477.
11. Rimola, A.; Costa, D.; Sodupe, M.; Lambert, J.-F.; Ugliengo, P., Silica Surface Features and Their Role in the Adsorption of Biomolecules: Computational Modeling and Experiments. *Chem. Rev.* **2013,** *113*, 4216-4313.
12. Remesal, E. R.; Amaya, J.; Graciani, J.; Márquez, A. M.; Sanz, J. F., Adsorption of prototypical amino acids on silica: Influence of the pre-adsorbed water multilayer. *Surf. Sci.* **2016,** *646*, 239-246.
13. Nonella, M.; Seeger, S., Investigating Alanine–Silica Interaction by Means of First-Principles Molecular-Dynamics Simulations. *ChemPhysChem* **2008,** *9*, 414-421.
14. Zhao, Y. L.; Köppen, S.; Frauenheim, T., An SCC-DFTB/MD Study of the Adsorption of Zwitterionic Glycine on a Geminal Hydroxylated Silica Surface in an Explicit Water Environment. *J. Phys. Chem. C* **2011,** *115*, 9615-9621.
15. Trachta, M.; Bludský, O.; Rubeš, M., The interaction of proteins with silica surfaces. Part I: Ab initio modeling. *Comput. Theor. Chem.* **2017,** *1117*, 100-107.
16. Rimola, A.; Corno, M.; Zicovich-Wilson, C. M.; Ugliengo, P., Ab Initio Modeling of Protein/Biomaterial Interactions: Glycine Adsorption at Hydroxyapatite Surfaces. *J. Am. Chem. Soc.* **2008,** *130*, 16181-16183.
17. Rimola, A.; Corno, M.; Zicovich-Wilson, C. M.; Ugliengo, P., Ab initio modeling of protein/biomaterial interactions: competitive adsorption between glycine and water onto hydroxyapatite surfaces. *Phys. Chem. Chem. Phys.* **2009,** *11*, 9005-9007.
18. Rimola, A.; Corno, M.; Garza, J.; Ugliengo, P., Ab initio modelling of protein–biomaterial interactions: influence of amino acid polar side chains on adsorption at hydroxyapatite surfaces. *Phil. Trans. R. Soc. A* **2012,** *370*, 1478-1498.
19. Pantaleone, S.; Rimola, A.; Sodupe, M., Canonical, Deprotonated, or Zwitterionic? A Computational Study on Amino Acid Interaction with the TiO2 (101) Anatase Surface. *J. Phys. Chem. C* **2017,** *121*, 14156-14165.
20. Pantaleone, S.; Rimola, A.; Sodupe, M., Canonical, deprotonated, or zwitterionic? II. A computational study on amino acid interaction with the TiO2(110) rutile surface: comparison with the anatase (101) surface. *Phys. Chem. Chem. Phys.* **2020,** *22*, 16862-16876.
21. Rimola, A.; Sodupe, M., Gas-Phase and Microsolvated Glycine Interacting with Boron Nitride Nanotubes. A B3LYP-D2* Periodic Study. **2014,** *2*, 334-350.
22. Fajín, J. L. C.; Gomes, J. R. B.; Cordeiro, M. N. D. S., DFT Study of the Adsorption of d-(l-)Cysteine on Flat and Chiral Stepped Gold Surfaces. *Langmuir* **2013,** *29*, 8856-8864.
23. Wang, M.-h.; Guo, Y.-n.; Wang, Q.; Zhang, X.-s.-y.; Huang, J.-j.; Lu, X.; Wang, K.-f.; Zhang, H.-p.; Leng, Y., Density functional theory study of interactions between glycine and TiO2/graphene nanocomposites. *Chem. Phys. Lett.* **2014,** *599*, 86-91.
24. Arrouvel, C.; Diawara, B.; Costa, D.; Marcus, P., DFT Periodic Study of the Adsorption of Glycine on the Anhydrous and Hydroxylated (0001) Surfaces of α-Alumina. *J. Phys. Chem. C* **2007,** *111*, 18164-18173.
25. Hong, G.; Heinz, H.; Naik, R. R.; Farmer, B. L.; Pachter, R., Toward Understanding Amino Acid Adsorption at Metallic Interfaces: A Density Functional Theory Study. *ACS Appl. Mater. Interf.* **2009,** *1*, 388-392.

26. Ghiringhelli, L. M.; Hess, B.; van der Vegt, N. F. A.; Delle Site, L., Competing Adsorption between Hydrated Peptides and Water onto Metal Surfaces: From Electronic to Conformational Properties. *J. Am. Chem. Soc.* **2008,** *130*, 13460-13464.
27. Iori, F.; Di Felice, R.; Molinari, E.; Corni, S., GolP: An atomistic force-field to describe the interaction of proteins with Au(111) surfaces in water. *Journal of Computational Chemistry* **2009,** *30*, 1465-1476.
28. Trachta, M.; Bludský, O.; Rubeš, M., The interaction of proteins with silica surfaces. Part II: Free energies of capped amino acids. *Comput. Theor. Chem.* **2019,** *1148*, 38-43.
29. Rimola, A., Intrinsic Ladders of Affinity for Amino-Acid-Analogues on Boron Nitride Nanomaterials: A B3LYP-D2* Periodic Study. *J. Phys. Chem. C* **2015,** *119*, 17707-17717.
30. Waters, K.; Pandey, R.; Karna, S. P., Amino Acid Analogue-Conjugated BN Nanomaterials in a Solvated Phase: First Principles Study of Topology-Dependent Interactions with a Monolayer and a (5,0) Nanotube. *ACS Omega* **2017,** *2*, 76-83.
31. Carravetta, V.; Monti, S., Peptide−TiO2 Surface Interaction in Solution by Ab Initio and Molecular Dynamics Simulations. *J. Phys. Chem. B* **2006,** *110*, 6160-6169.
32. Wright, L. B.; Rodger, P. M.; Corni, S.; Walsh, T. R., GolP-CHARMM: First-Principles Based Force Fields for the Interaction of Proteins with Au(111) and Au(100). *J. Chem. Theory Comput.* **2013,** *9*, 1616-1630.
33. Wright, L. B.; Rodger, P. M.; Walsh, T. R.; Corni, S., First-Principles-Based Force Field for the Interaction of Proteins with Au(100)(5 × 1): An Extension of GolP-CHARMM. *J. Phys. Chem. C* **2013,** *117*, 24292-24306.
34. Siwko, M. E.; Corni, S., Cytochrome C on a gold surface: investigating structural relaxations and their role in protein–surface electron transfer by molecular dynamics simulations. *Phys. Chem. Chem. Phys.* **2013,** *15*, 5945-5956.
35. Zanetti-Polzi, L.; Daidone, I.; Bortolotti, C. A.; Corni, S., Surface Packing Determines the Redox Potential Shift of Cytochrome c Adsorbed on Gold. *J. Am. Chem. Soc.* **2014,** *136*, 12929-12937.
36. Ghosh, S.; Jana, S.; Guchhait, N., Domain Specific Association of Small Fluorescent Probe trans-3-(4-Monomethylaminophenyl)-Acrylonitrile (MMAPA) with Bovine Serum Albumin (BSA) and Its Dissociation from Protein Binding Sites by Ag Nanoparticles: Spectroscopic and Molecular Docking Study. *J. Phys. Chem. B* **2012,** *116*, 1155-1163.
37. Aliaga, A. E.; Ahumada, H.; Sepúlveda, K.; Gomez-Jeria, J. S.; Garrido, C.; Weiss-López, B. E.; Campos-Vallette, M. M., SERS, Molecular Dynamics and Molecular Orbital Studies of the MRKDV Peptide on Silver and Membrane Surfaces. *J. Phys. Chem. C* **2011,** *115*, 3982-3989.
38. Kang, Y.; Li, X.; Tu, Y.; Wang, Q.; Ågren, H., On the Mechanism of Protein Adsorption onto Hydroxylated and Nonhydroxylated TiO2 Surfaces. *J. Phys. Chem. C* **2010,** *114*, 14496-14502.
39. Wu, C.; Chen, M.; Skelton, A. A.; Cummings, P. T.; Zheng, T., Adsorption of Arginine–Glycine–Aspartate Tripeptide onto Negatively Charged Rutile (110) Mediated by Cations: The Effect of Surface Hydroxylation. *ACS Appl. Mater. Interf.* **2013,** *5*, 2567-2579.
40. Wright, L. B.; Walsh, T. R., Efficient conformational sampling of peptides adsorbed onto inorganic surfaces: insights from a quartz binding peptide. *Phys. Chem. Chem. Phys.* **2013,** *15*, 4715-4726.
41. Schneider, J.; Ciacchi, L. C., A Classical Potential to Model the Adsorption of Biological Molecules on Oxidized Titanium Surfaces. *J. Chem. Theory Comput.* **2011,** *7*, 473-484.
42. Patwardhan, S. V.; Emami, F. S.; Berry, R. J.; Jones, S. E.; Naik, R. R.; Deschaume, O.; Heinz, H.; Perry, C. C., Chemistry of Aqueous Silica Nanoparticle Surfaces and the Mechanism of Selective Peptide Adsorption. *J. Am. Chem. Soc.* **2012,** *134*, 6244-6256.
43. Boughton, A. P.; Andricioaei, I.; Chen, Z., Surface Orientation of Magainin 2: Molecular Dynamics Simulation and Sum Frequency Generation Vibrational Spectroscopic Studies. *Langmuir* **2010,** *26*, 16031-16036.

44. Wei, T.; Carignano, M. A.; Szleifer, I., Lysozyme Adsorption on Polyethylene Surfaces: Why Are Long Simulations Needed? *Langmuir* **2011,** *27*, 12074-12081.
45. Liu, J.; Liao, C.; Zhou, J., Multiscale Simulations of Protein G B1 Adsorbed on Charged Self-Assembled Monolayers. *Langmuir* **2013,** *29*, 11366-11374.
46. Mücksch, C.; Urbassek, H. M., Molecular Dynamics Simulation of Free and Forced BSA Adsorption on a Hydrophobic Graphite Surface. *Langmuir* **2011,** *27*, 12938-12943.
47. Raffaini, G.; Ganazzoli, F., Surface Topography Effects in Protein Adsorption on Nanostructured Carbon Allotropes. *Langmuir* **2013,** *29*, 4883-4893.
48. Sun, X.; Feng, Z.; Hou, T.; Li, Y., Mechanism of Graphene Oxide as an Enzyme Inhibitor from Molecular Dynamics Simulations. *ACS Appl. Mater. Interf.* **2014,** *6*, 7153-7163.
49. Balamurugan, K.; Gopalakrishnan, R.; Raman, S. S.; Subramanian, V., Exploring the Changes in the Structure of α-Helical Peptides Adsorbed onto a Single Walled Carbon Nanotube Using Classical Molecular Dynamics Simulation. *J. Phys. Chem. B* **2010,** *114*, 14048-14058.
50. Kraszewski, S.; Tarek, M.; Treptow, W.; Ramseyer, C., Affinity of C60 Neat Fullerenes with Membrane Proteins: A Computational Study on Potassium Channels. *ACS Nano* **2010,** *4*, 4158-4164.
51. Gray, J. J., The interaction of proteins with solid surfaces. *Curr. Opin. Struct. Biol.* **2004,** *14*, 110-115.
52. Salata, O. V., Applications of nanoparticles in biology and medicine. *J. Nanobiotech.* **2004,** *2*, 3.
53. Wong, I. Y.; Bhatia, S. N.; Toner, M., Nanotechnology: emerging tools for biology and medicine. *Genes Dev.* **2013,** *27*, 2397-2408.
54. Yao, J.; Yang, M.; Duan, Y., Chemistry, Biology, and Medicine of Fluorescent Nanomaterials and Related Systems: New Insights into Biosensing, Bioimaging, Genomics, Diagnostics, and Therapy. *Chem. Rev.* **2014,** *114*, 6130-6178.
55. Balasundaram, G.; Webster, T. J., Nanotechnology and biomaterials for orthopedic medical applications. *Nanomedicine* **2006,** *1*, 169-176.
56. James Cleaves Ii, H.; Michalkova Scott, A.; Hill, F. C.; Leszczynski, J.; Sahai, N.; Hazen, R., Mineral–organic interfacial processes: potential roles in the origins of life. *Chem. Soc. Rev.* **2012,** *41*, 5502-5525.
57. Rimola, A.; Sodupe, M.; Ugliengo, P., Role of Mineral Surfaces in Prebiotic Chemical Evolution. In Silico Quantum Mechanical Studies. **2019,** *9*, 10.
58. Bernal, J. D., The Physical Basis of Life. *Proc. Phys. Soc. B* **1949,** *62*, 597-618.
59. Orgel, L. E., Polymerization on the Rocks: Theoretical Introduction. *Orig. Life Evol. Biosph.* **1998,** *28*, 227-234.
60. Smith, J. V., Biochemical evolution. I. Polymerization on internal, organophilic silica surfaces of dealuminated zeolites and feldspars. *Proc. Natl. Acad. Sci. USA* **1998,** *95*, 3370.
61. Hazen, R. M., Mineral surfaces and the prebiotic selection and organization of biomolecules. *Am. Mineral.* **2006,** *91*, 1715-1729.
62. Wächtershäuser, G., Evolution of the first metabolic cycles. *Proc. Natl. Acad. Sci. USA* **1990,** *87*, 200.
63. Cody, G. D.; Boctor, N. Z.; Filley, T. R.; Hazen, R. M.; Scott, J. H.; Sharma, A.; Yoder, H. S., Primordial Carbonylated Iron-Sulfur Compounds and the Synthesis of Pyruvate. *Science* **2000,** *289*, 1337.
64. Muchowska, K. B.; Varma, S. J.; Moran, J., Synthesis and breakdown of universal metabolic precursors promoted by iron. *Nature* **2019,** *569*, 104-107.
65. Huber, C.; Eisenreich, W.; Hecht, S.; Wächtershäuser, G., A Possible Primordial Peptide Cycle. *Science* **2003,** *301*, 938.
66. Ferrari, A. M.; Civalleri, B.; Dovesi, R., Ab initio periodic study of the conformational behavior of glycine helical homopeptides. *J. Comput. Chem.* **2010,** *31*, 1777-1784.
67. Cutini, M.; Corno, M.; Ugliengo, P., Method Dependence of Proline Ring Flexibility in the Poly-l-Proline Type II Polymer. *J. Chem. Theory Comput.* **2017,** *13*, 370-379.

68. Cutini, M.; Bocus, M.; Ugliengo, P., Decoding Collagen Triple Helix Stability by Means of Hybrid DFT Simulations. *J. Phys. Chem. B* **2019,** *123*, 7354-7364.
69. Cutini, M.; Pantaleone, S.; Ugliengo, P., Elucidating the Nature of Interactions in Collagen Triple-Helix Wrapping. *J. Phys. Chem. Lett.* **2019,** *10*, 7644-7649.
70. Cutini, M.; Bechis, I.; Corno, M.; Ugliengo, P., Balancing Cost and Accuracy in Quantum Mechanical Simulations on Collagen Protein Models. *J. Chem. Theory Comput.* **2021,** *17*, 2566-2574.
71. Cutini, M.; Corno, M.; Costa, D.; Ugliengo, P., How Does Collagen Adsorb on Hydroxyapatite? Insights From Ab Initio Simulations on a Polyproline Type II Model. *J. Phys. Chem. C* **2019,** *123*, 7540-7550.
72. Ali, I.; Suhail, M.; Alothman, Z. A.; Alwarthan, A., Recent advances in syntheses, properties and applications of TiO2 nanostructures. *RSC Adv.* **2018,** *8*, 30125-30147.
73. Jafari, S.; Mahyad, B.; Hashemzadeh, H.; Janfaza, S.; Gholikhani, T.; Tayebi, L., Biomedical Applications of TiO(2) Nanostructures: Recent Advances. *Int. J. Nanomedicine* **2020,** *15*, 3447-3470.
74. Wu, W.-h.; Sun, X.; Yu, Y.-p.; Hu, J.; Zhao, L.; Liu, Q.; Zhao, Y.-f.; Li, Y.-m., TiO2 nanoparticles promote β-amyloid fibrillation in vitro. *Biochem. Biophys. Res. Commun.* **2008,** *373*, 315-318.
75. Wu, X.; Narsimhan, G., Effect of surface concentration on secondary and tertiary conformational changes of lysozyme adsorbed on silica nanoparticles. *Biochim. Biophys. Acta* **2008,** *1784*, 1694-1701.
76. Nelson, R.; Sawaya, M. R.; Balbirnie, M.; Madsen, A. Ø.; Riekel, C.; Grothe, R.; Eisenberg, D., Structure of the cross-β spine of amyloid-like fibrils. *Nature* **2005,** *435*, 773-778.
77. Martra, G.; Deiana, C.; Sakhno, Y.; Barberis, I.; Fabbiani, M.; Pazzi, M.; Vincenti, M., The Formation and Self-Assembly of Long Prebiotic Oligomers Produced by the Condensation of Unactivated Amino Acids on Oxide Surfaces. *Angew. Chem. Int. Ed.* **2014,** *53*, 4671-4674.
78. Pantaleone, S.; Ugliengo, P.; Sodupe, M.; Rimola, A., When the Surface Matters: Prebiotic Peptide-Bond Formation on the TiO2 (101) Anatase Surface through Periodic DFT-D2 Simulations. *Chem. Eur. J.* **2018,** *24*, 16292-16301.
79. Liu, Z.; Hinaut, A.; Peeters, S.; Scherb, S.; Meyer, E.; Righi, M. C.; Glatzel, T., Reconstruction of a 2D layer of KBr on Ir(111) and electromechanical alteration by graphene. *Beilstein J. Nanotechnol.* **2021,** *12*, 432-439.
80. Restuccia, P.; Righi, M. C., Tribochemistry of graphene on iron and its possible role in lubrication of steel. *Carbon* **2016,** *106*, 118-124.
81. Burdett, J. K.; Hughbanks, T.; Miller, G. J.; Richardson, J. W.; Smith, J. V., Structural-electronic relationships in inorganic solids: powder neutron diffraction studies of the rutile and anatase polymorphs of titanium dioxide at 15 and 295 K. *J. Am. Chem. Soc.* **1987,** *109*, 3639-3646.
82. Kresse, G.; Hafner, J., Ab initio molecular dynamics for liquid metals. *Phys. Rev. B* **1993,** *47*, 558-561.
83. Kresse, G.; Hafner, J., Ab initio molecular-dynamics simulation of the liquid-metal--amorphous-semiconductor transition in germanium. *Phys. Rev. B* **1994,** *49*, 14251-14269.
84. Kresse, G.; Furthmüller, J., Efficient iterative schemes for ab initio total-energy calculations using a plane-wave basis set. *Phys. Rev. B* **1996,** *54*, 11169-11186.
85. Kresse, G.; Furthmüller, J., Efficiency of ab-initio total energy calculations for metals and semiconductors using a plane-wave basis set. *Comput. Mater. Sci.* **1996,** *6*, 15-50.
86. Kresse, G.; Joubert, D., From ultrasoft pseudopotentials to the projector augmented-wave method. *Phys. Rev. B* **1999,** *59*, 1758-1775.
87. Perdew, J. P.; Burke, K.; Ernzerhof, M., Generalized Gradient Approximation Made Simple. *Phys. Rev. Lett.* **1996,** *77*, 3865-3868.
88. Grimme, S., Semiempirical GGA-type density functional constructed with a long-range dispersion correction. *J. Comput. Chem.* **2006,** *27*, 1787-1799.

89. Civalleri, B.; Zicovich-Wilson, C. M.; Valenzano, L.; Ugliengo, P., B3LYP augmented with an empirical dispersion term (B3LYP-D*) as applied to molecular crystals. *CrystEngComm* **2008,** *10*, 405-410.
90. Mathew, K.; Sundararaman, R.; Letchworth-Weaver, K.; Arias, T. A.; Hennig, R. G., Implicit solvation model for density-functional study of nanocrystal surfaces and reaction pathways. *J. Chem. Phys.* **2014,** *140*, 084106.
91. Mathew, K.; Kolluru, V. S. C.; Mula, S.; Steinmann, S. N.; Hennig, R. G., Implicit self-consistent electrolyte model in plane-wave density-functional theory. *J. Chem. Phys.* **2019,** *151*, 234101.
92. González, D.; Heras-Domingo, J.; Pantaleone, S.; Rimola, A.; Rodríguez-Santiago, L.; Solans-Monfort, X.; Sodupe, M., Water Adsorption on MO_2 (M = Ti, Ru, and Ir) Surfaces. Importance of Octahedral Distortion and Cooperative Effects. *ACS Omega* **2019,** *4*, 2989-2999.
93. Yasuda, S.; Yoshidome, T.; Oshima, H.; Kodama, R.; Harano, Y.; Kinoshita, M., Effects of side-chain packing on the formation of secondary structures in protein folding. *J. Chem. Phys.* **2010,** *132*, 065105.
94. Chellgren, B. W.; Creamer, T. P., Side-chain entropy effects on protein secondary structure formation. *Proteins* **2006,** *62*, 411-420.

Table 1. Calculated total adsorption energies (ΔE_{ADS}) and adsorption energy normalized per amino acidic unit ($\Delta E_{ADS/unit}$) for each studied complex, both in the gas phase and under PCM conditions. Other energetic terms of interest are also included: is the energetic gain due to the secondary structure formation with respect to the extended primary polyglycine structure ($\Delta E_{H/unit}$), the deformation energy of the secondary structure due to the adsorption ($\Delta E_{def/unit}$), and the sum of these two terms ($\Delta E_{H+def/unit}$). See the Methods section for more details on these terms. Energy units are in kJ mol^{-1}.

System	AA units	Gas-phase					PCM				
		ΔE_{ADS}	$\Delta E_{ADS/uni}$	$\Delta E_{H/unit}$	$\Delta E_{def/uni}$	$\Delta E_{H+def/}$	ΔE_{ADS}	$\Delta E_{ADS/uni}$	$\Delta E_{H/unit}$	$\Delta E_{def/uni}$	$\Delta E_{H+def/}$
extended/TiO_2	2	-62.0	-31.0	0.0	15.3	15.3	-3.8	-1.9	0.0	13.7	13.7
β-sheet_AP/TiO_2	4	-120.8	-30.2	-23.6	23.0	-0.6	-0.5	-0.1	-9.1	19.7	10.6
β-sheet_P/TiO_2	4	-115.6	-28.9	-18.5	19.6	1.1	-3.6	-0.9	-3.8	13.8	10.0
β-sheet_BRK/TiO_2	4	-123.2	-30.8	0.0	11.8	11.8	-16.4	-4.1	0.0	10.4	10.4
α-helix_1/TiO_2	7	-220.5	-31.5	-21.5	8.6	12.9	-84.1	-12.0	-9.9	5.9	-4.0
α-helix_2/TiO_2	7	-235.9	-33.7	-21.5	14.1	7.4	-80.8	-11.5	-9.9	9.4	-0.5

Table 2. Energy terms for the interaction of β-sheet_AP and β-sheet_P with the TiO_2 (101) anatase surface. E1 is the interaction between P1 and S (the strand where Ti-O bonds are present), E2 is the interaction between P2 and S (the strand with dispersion forces only), $E_{H\text{-}bond}$ is the interaction energy of the H-bond pattern. E_{CALC} is the sum of all the systems separately and their interaction energies, *i.e.*, $E_{P1} + E_{P2} + E_S + E1 + E2 + E_{H\text{-}bond}$ (see the Methods section for more details). E_{TOT} is the absolute total energy of the systems provided by VASP. $|\Delta E|$ is the difference in energy between E_{CALC} and E_{TOT}. Units are in kJ mol^{-1}.

System	E1	E2	$E_{H\text{-}bond}$	E_{CALC}	E_{TOT}	$\|\Delta E\|$
β-sheet_AP	-111.1	-35.1	-79.6	-80095.9	-80094.9	1.0
β-sheet_P	-113.7	-33.2	-73.1	-80090.1	-80089.8	0.3

Table 3. Values of the reaction energies (in kJ/mol) of the α-helix → β-sheet conformational change of the isolated secondary structures$\Delta\Delta E_{iso/unit}$ and on the TiO_2 (101) anatase surface ($\Delta\Delta E_{surf/unit}$), including the involved energy terms according to the energy cycles shown in Figure 4 ($\Delta\Delta E_{surf/unit} = \Delta E^{(\beta)}_{ADS/unit} - \Delta E^{(\alpha)}_{ADS/unit} + \Delta\Delta E_{iso/unit}$), both in the gas phase and in implicit PCM water solvent. See the text and SI for details on the definition of the energy terms.

Reaction	Conditions	$\Delta E^{(\beta)}_{ADS/unit}$	$\Delta E^{(\alpha)}_{ADS/unit}$	$\Delta\Delta E_{iso/unit}$	$\Delta\Delta E_{surf/unit}$
α-helix_2 → β-sheet_AP	Gas-phase	-6.6	-12.2	-2.1	1.2
	PCM	9.0	-1.6	0.8	11.9
α-helix_2 → β-sheet_P	Gas-phase	-10.4	-12.2	3.0	2.5
	PCM	2.9	-1.6	6.1	11.1
α-helix_1 → β-sheet_AP	Gas-phase	-6.6	-9.9	-2.1	1.2
	PCM	9.0	-2.1	0.8	11.9
α-helix_1 → β-sheet_P	Gas-phase	-10.4	-9.9	3.0	2.5
	PCM	2.9	-2.1	6.1	11.1

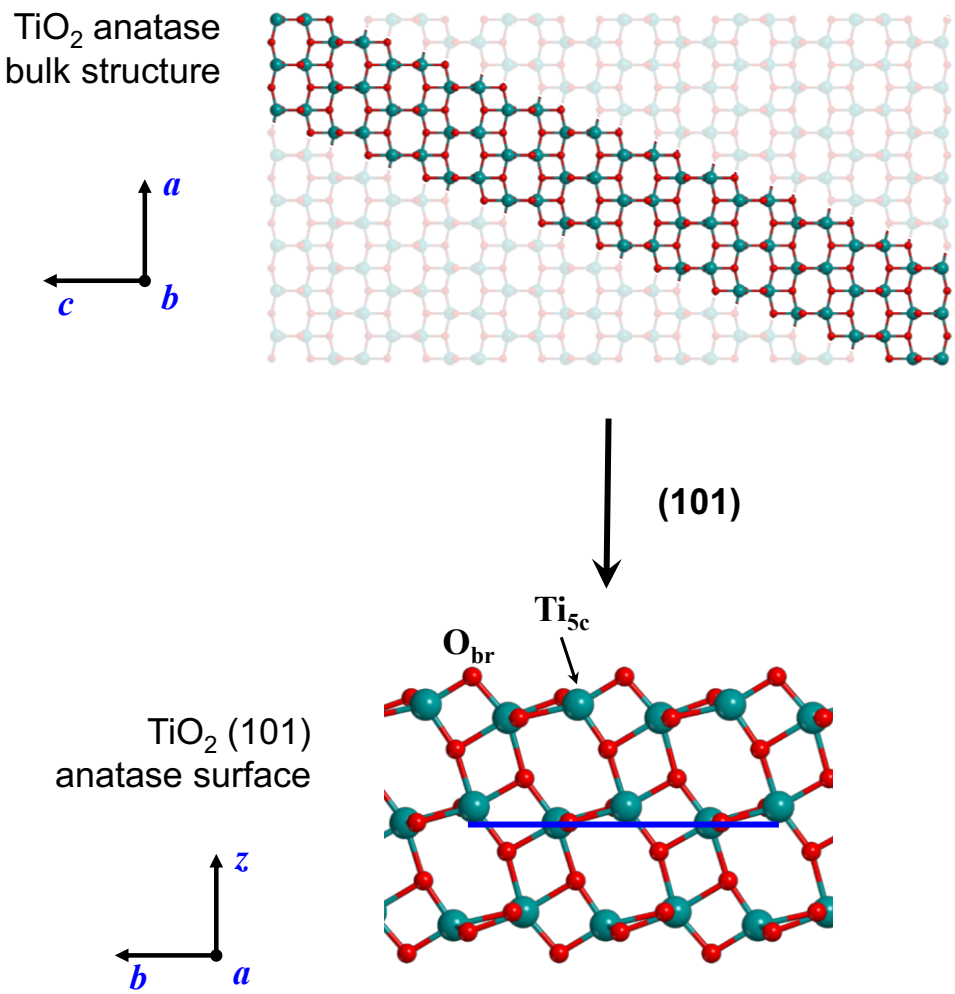

Figure 1. Crystalline models for the TiO_2 anatase bulk structure and the TiO_2 (101) anatase surface model, representing the process of cutting out the bulk structure to construct the surface. The unit cell of the surface (along the *b* axis) is represented in blue.

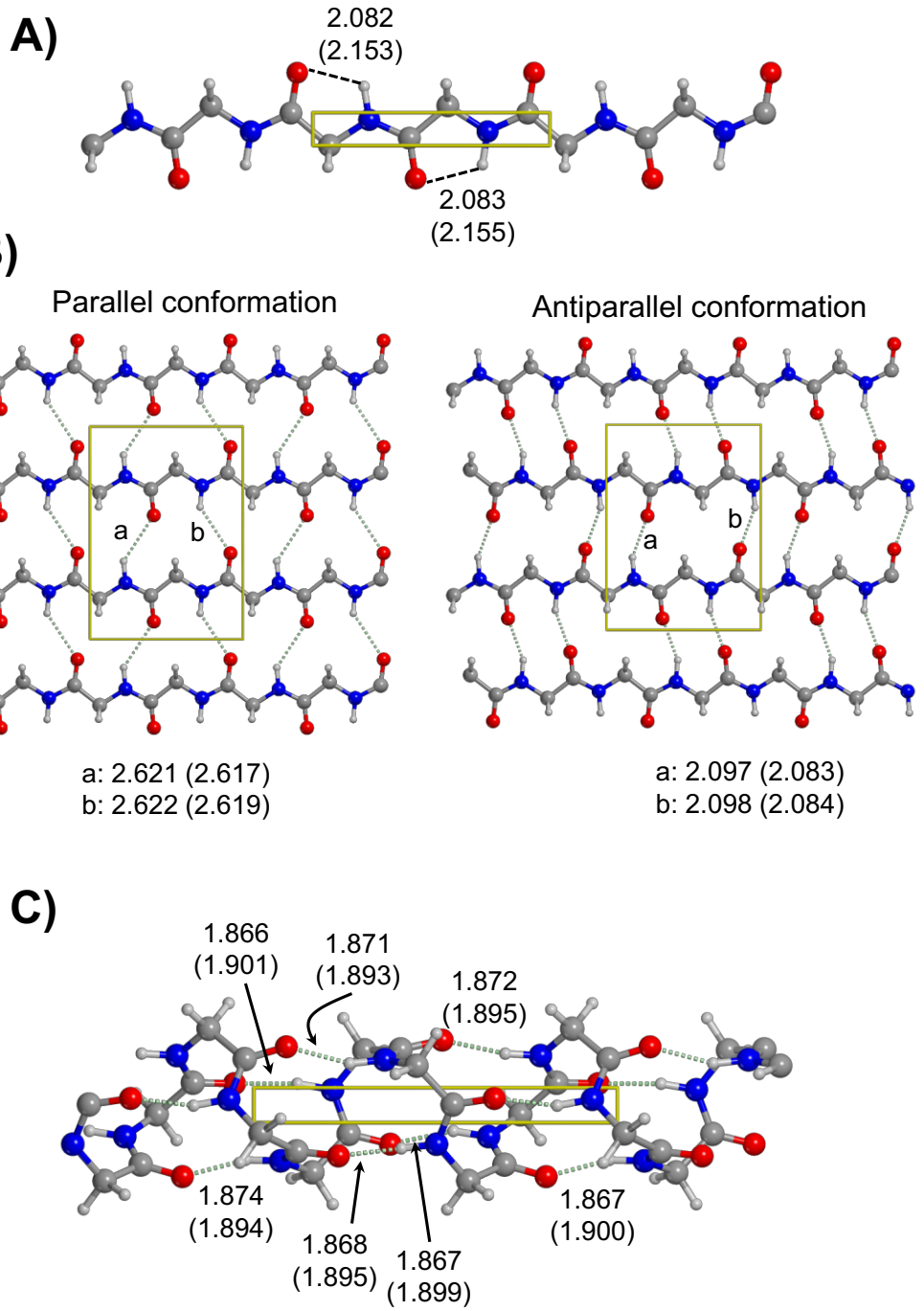

Figure 2. PBE-D2* optimized geometries for the isolated periodic polyglycine structures: A) extended primary, B) β-sheet (parallel and antiparallel conformations) and C) α-helix. Bond distances are in Å. Bare values refer to distances for optimized structures in the gas phase, while values in parenthesis for those optimized with PCM. The unit cells are represented in yellow. Atom colour legend: white, hydrogen; grey, carbon; blue, nitrogen; red, oxygen.

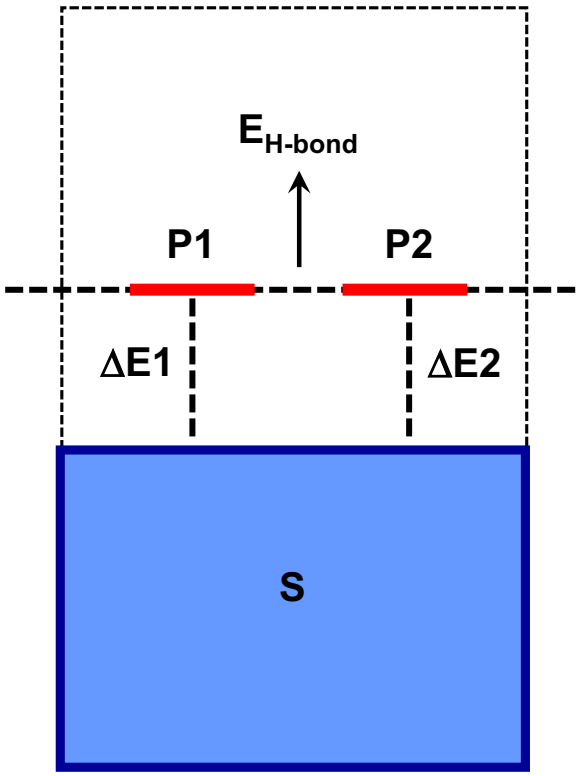

Figure 3. Schematic representation of the β-sheet/TiO_2 complexes and the interactions involved. See text for details.

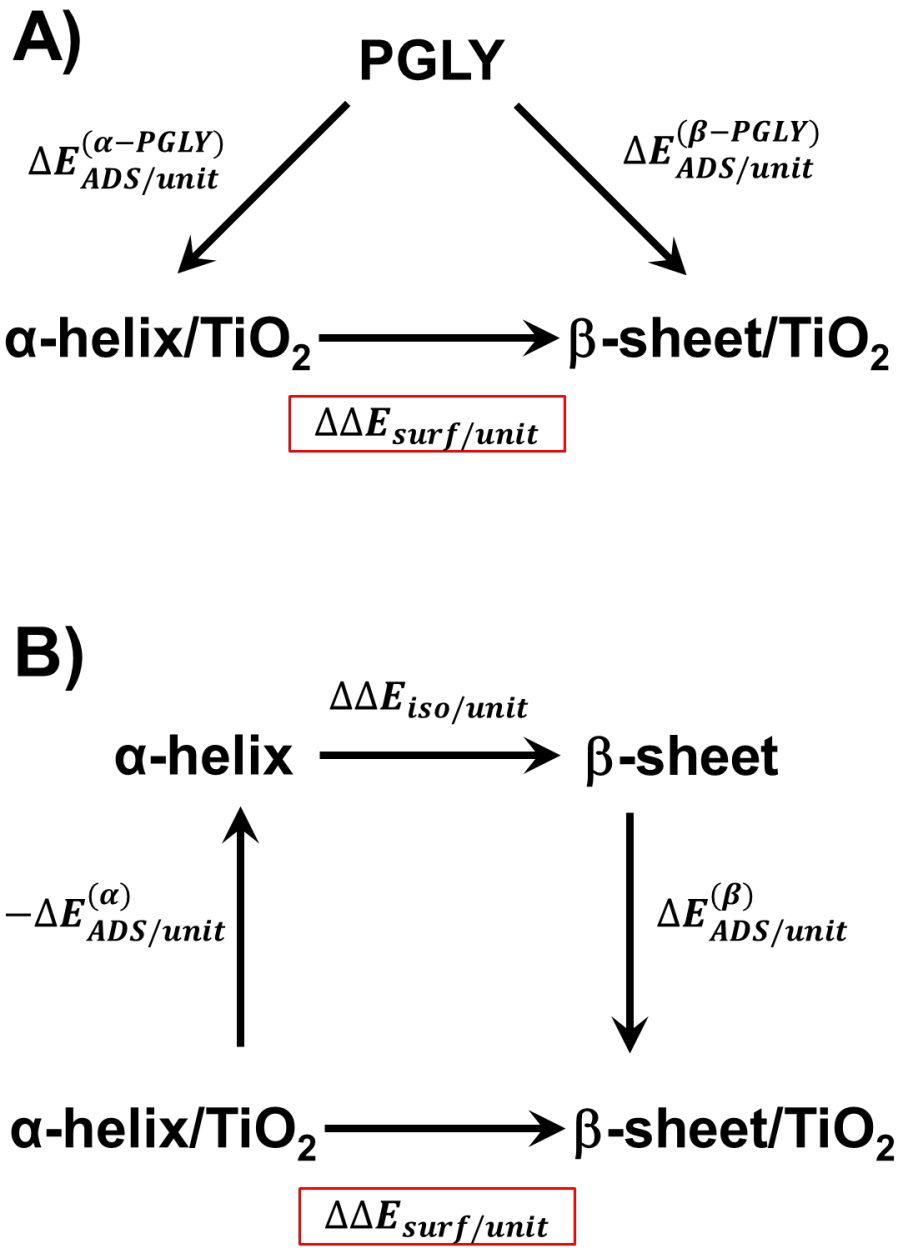

Figure 4. Energy cycles to compute the reaction energy associated with the conversion process of α-helix/TiO_2 → β-sheet/TiO_2: A) based on the energy balance between the normalized adsorption energies of the α-helix and β-sheet to the surfaces from the periodic isolated extended primary polyglycine structure ($\Delta\Delta E_{surf/unit} = \Delta E_{ADS/unit}^{(\beta-PGLY)} - \Delta E_{ADS/unit}^{(\alpha-PGLY)}$); B) based on an energy cycle adopting a three-step process: i) desorption of the α-helix from the surface into its periodic isolated state, ii) conformational change from α-helix to β-sheet in their periodic isolated states, and iii) adsorption of the β-sheet to the surface from its periodic isolated state ($\Delta\Delta E_{surf/unit} = \Delta E_{ADS/unit}^{(\beta)} - \Delta E_{ADS/unit}^{(\alpha)} + \Delta\Delta E_{iso/unit}$).

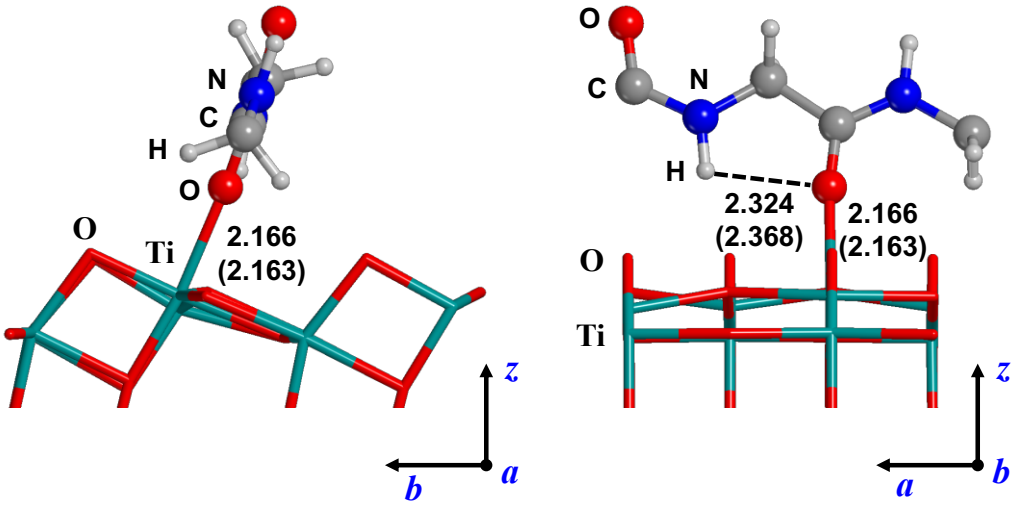

Figure 5. PBE-D2* optimized structure of the extended/TiO_2 complex, along the *a* (left) and *b* (right) axes. Distances are in Å. Bare numbers refer to distances in the gas phase, while those in parenthesis to values with implicit solvation.

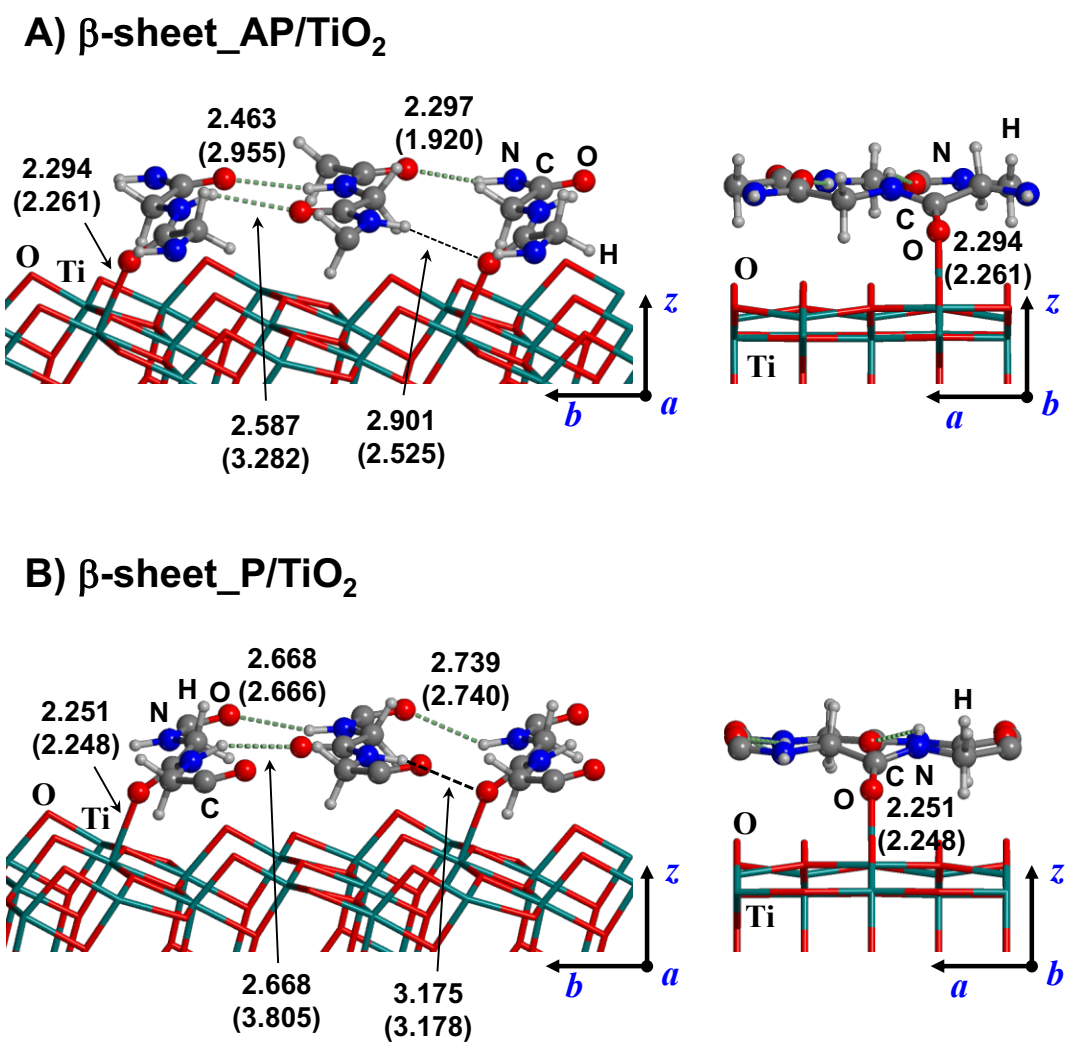

Figure 6. PBE-D2* optimized structures of the β-sheet/TiO_2 complexes, adopting the antiparallel (A) and the parallel (B) conformations. Distances are in Å. Bare numbers refer to distances in the gas phase, while those in parenthesis to values with implicit solvation.

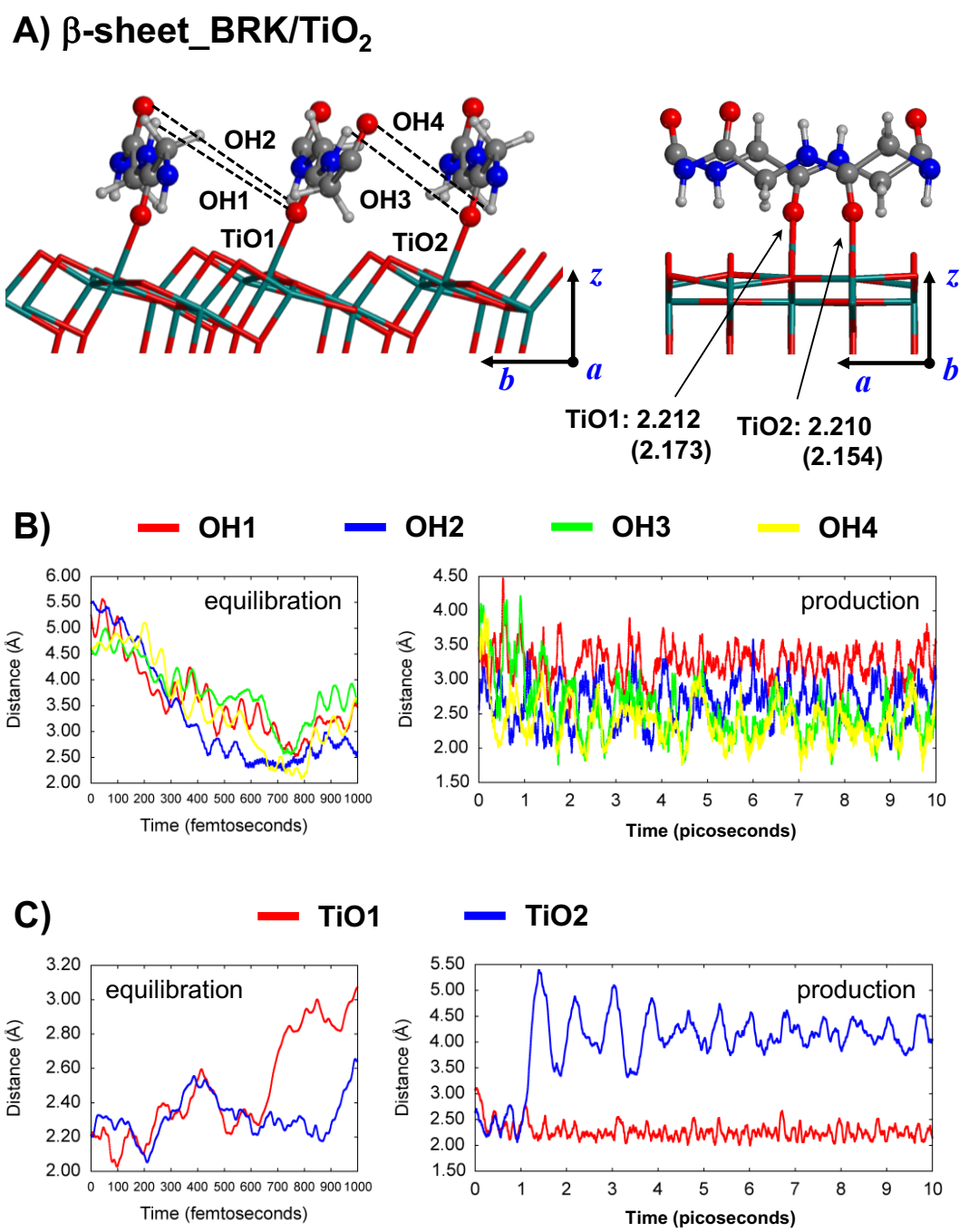

Figure 7. A) PBE-D2* optimized structure of the β-sheet_BRK/TiO_2 complex, Distances are in Å. Bare numbers refer to distances in the gas phase, while those in parenthesis to values with implicit solvation. Evolution of the H-bonds (B) and of the Ti—O distances (C) during the AIMD simulations, in both the equilibration and the production periods. Atom colour legend: white, hydrogen; grey, carbon; blue, nitrogen; red, oxygen; cyan, titanium.

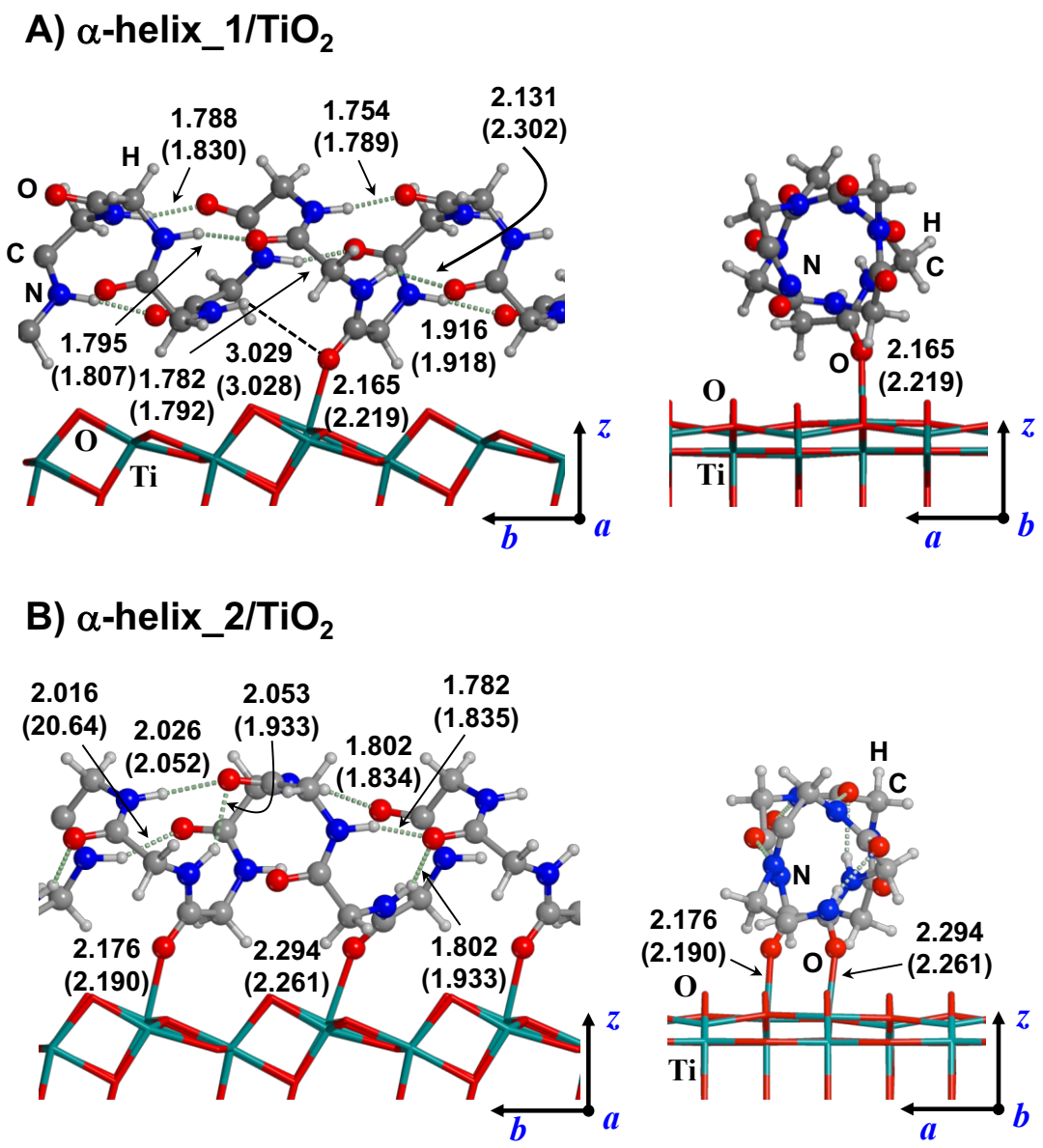

Figure 8. PBE-D2* optimized structures of the α-helix_1/TiO_2 (A) and α-helix_2/TiO_2 (B) complexes. Distances are in Å. Bare numbers refer to distances in the gas phase, while those in parenthesis to values with implicit solvation.

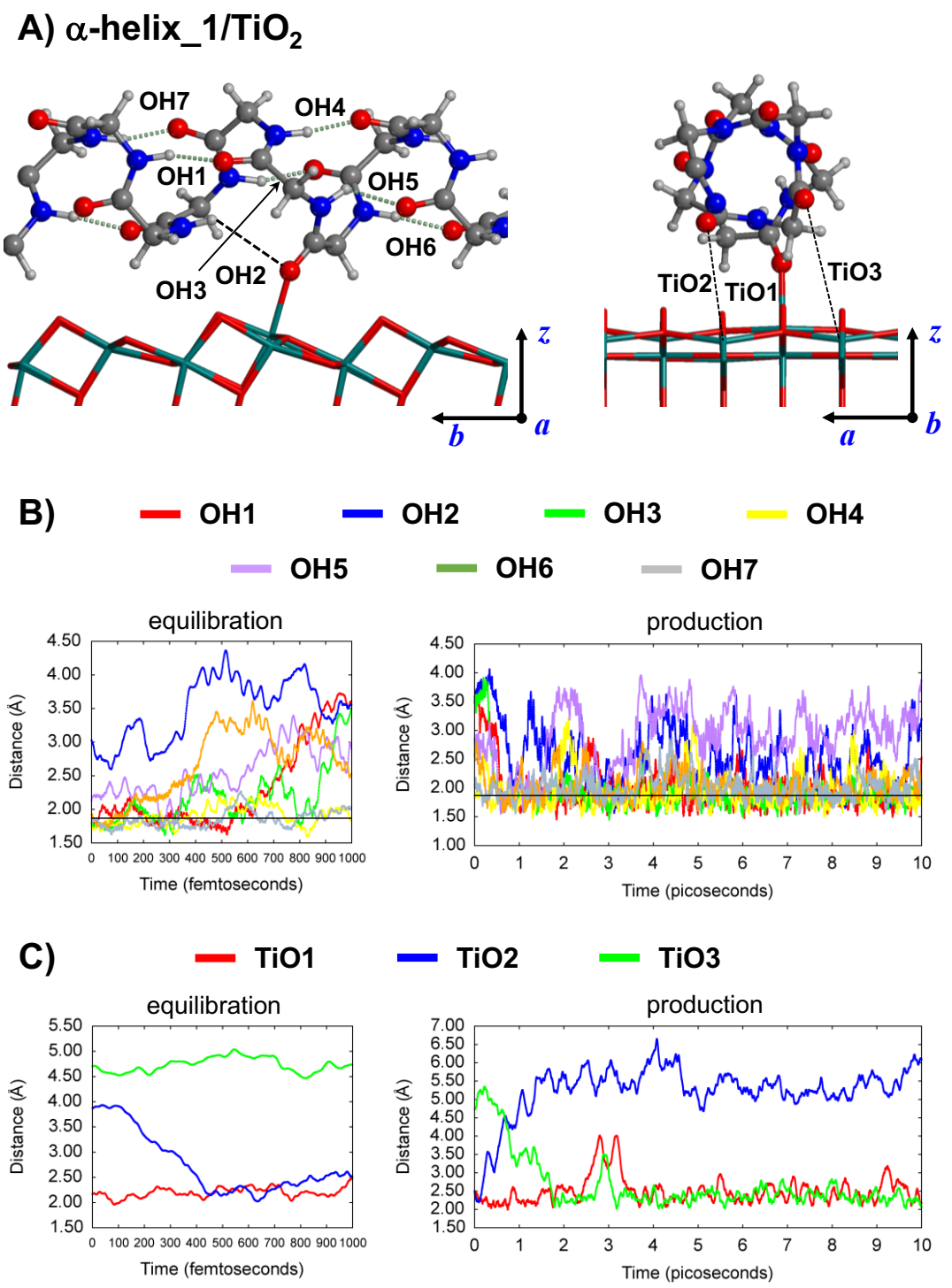

Figure 9. A) H-bond patterns and Ti-O distances present in the α-helix_1/TiO_2 complex Evolution of these H-bonds (B) and of the Ti—O distances (C) during the AIMD simulations, in both the equilibration and the production periods. Atom colour legend: white, hydrogen; grey, carbon; blue, nitrogen; red, oxygen; cyan, titanium.

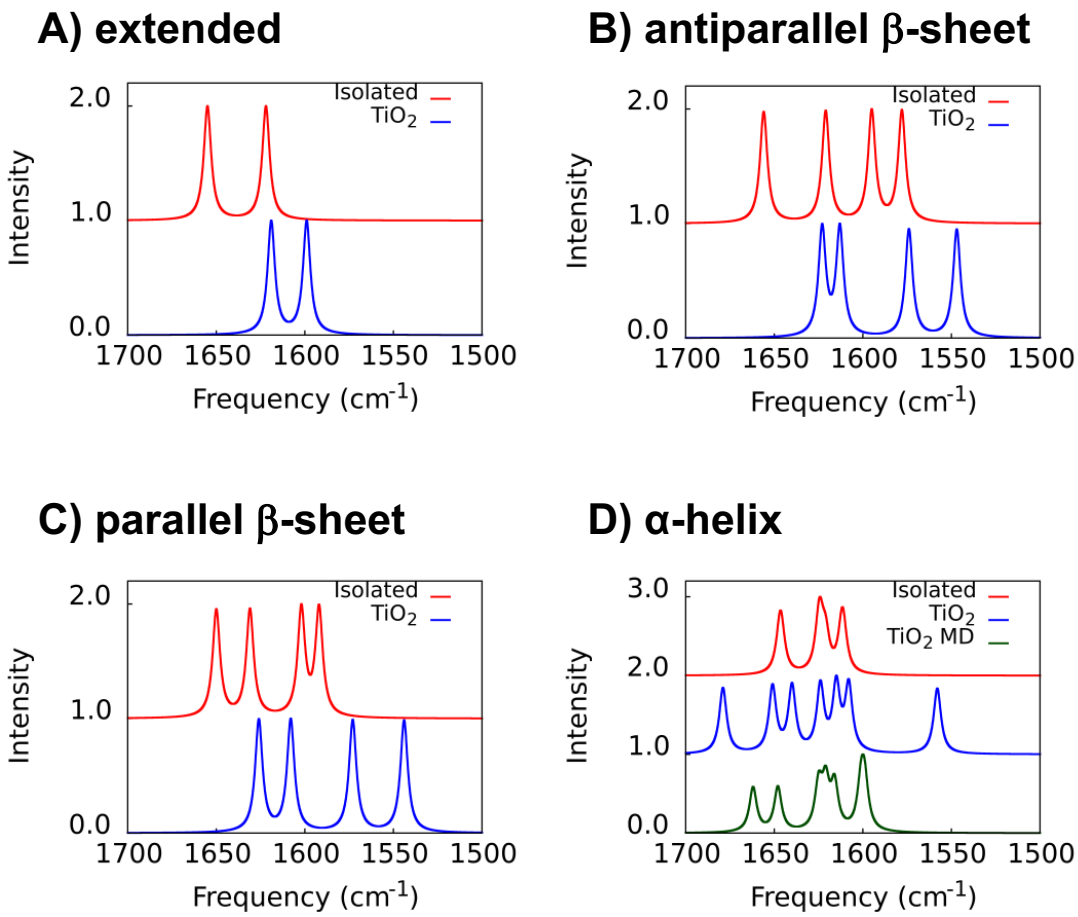

Figure 10. IR-spectra of the CO vibration for the secondary structures analysed in this work, both in the isolated state and as adsorbed on the TiO_2 surface. Intensities (in arbitrary units) were normalized to 1.